Ore Geology Reviews 144 (2022) 104813

Contents lists available at ScienceDirect

Ore Geology Reviews

journal homepage: www.elsevier.com/locate/oregeorev

Diagenesis of Ediacaran – early Cambrian phosphorite: Comparisons with recent phosphate sediments based on LA-ICP-MS and EMPA

Haiying Yang [a,b,c], Jiafei Xiao [b,*], Yong Xia [b], Zhifang Zhao [a,c,d,e,*], Zhuojun Xie [b], Shan He [b], Shengwei Wu [b]

[a] School of Earth Sciences, Yunnan University, Kunming 650500, China
[b] State Key Laboratory of Ore Deposit Geochemistry, Institute of Geochemistry, Chinese Academy of Sciences, Guiyang 550081, China
[c] Institute of International River and Eco-security, Yunnan University, Kunming 650500, China
[d] Research Center of Domestic High-resolution Satellite Remote Sensing Geological Engineering, University of Yunnan Province, Kunming 650500, China
[e] MNR Key Laboratory of Sanjiang Metallogeny and Resources Exploration & Utilization, Kunming 650051, China

ARTICLE INFO

Keywords:
Ediacaran-early Cambrian
Old phosphorite
Diagenesis
In situ geochemistry
Recent apatites

ABSTRACT

"Old phosphorite" deposits (Ediacaran to early Cambrian) located in Central Guizhou, South China, are hosted in carbonate and represent the earliest phosphogenesis. These old phosphorites, as well as Pliocene to Pleistocene and modern phosphate sediments (recent phosphorite) have been extensively studied. However, the possibility of recent phosphorite being the incipient stage of long-time phosphorite remains uncertain. Taking Weng'an (Ediacaran) and Zhijin (early Cambrian) phosphorites as examples, this study conducted in situ geochemical and mineralogical analyses of phosphate minerals (old apatites). Analogies between recent and old apatites were determined by comparing geochemistry based on rare earth elements (REE) and yttrium (REE + Y). Old phosphorite could be divided into authigenic grains and biodetritus, both comprising closely accumulated apatite nanocrystals. REE + Y concentrations (∑REE + Y) were much higher in the outer rim than in the inner core of biodetritus, whereas the authigenic grains showed relatively homogeneous REE + Y distributions. Three REE + Y patterns were observed: (1) "left-inclined" type, with no Ce anomalies; (2) shale-like pattern, with weak MREE enrichment and slightly negative Ce anomalies; (3) "hat-shaped" pattern, with notable MREE enrichment, evident HREE depletion, and remarkable negative Ce anomalies. Positive La, Gd, and Y anomalies, as well as MREE enrichment increased from type (1) to type (3), which can be explained by increasing degrees of oxidation. The REE + Y distributions of old apatites were similar to those of recent apatites, but exhibited MREE enrichment and HREE depletion and old authigenic apatites had no Ce anomalies. Furthermore, old apatite compositions lie in the diagenetic area on Y/Ho vs Sm_N/Yd_N plots. These characteristics indicate that old phosphorite could have been subjected to long-term diagenetic modification after burial, during which apatites recrystallized and absorbed REE + Y. Hence, it can be concluded that recent apatites could serve as predecessors of major ancient phosphorite, especially biogenic phosphorites. Globally, typical old phosphorites have quite variable REE + Y compositions, suggesting that the phosphorites experienced different depositional conditions and diagenetic alteration despite their contemporaneous formation. This study provides new data and insight on the diagenesis of old phosphorite and improves our deeper understanding of phosphogenesis in paleo- and modern environments.

1. Introduction

Marine sedimentary phosphorite represents the most widespread phosphate rock resources. The most important deposits formed during the Precambrian–Cambrian transition, including the Ediacaran (~635–541 Ma) and early Cambrian (~541–529) phases (Cook and Shergold, 1984; Pufahl and Groat, 2017). These deposits represent the earliest phosphogenesis (Cook and Shergold, 1984; Cook, 1992; Pufahl and Groat, 2017) and are called "old phosphorite" (Ilyin, 1998). Phosphogenesis occurred soon after the Marinoan glaciation (Papineau, 2010; Planavsky et al., 2010), leading to the wide distribution of phosphorites in Asia, Australia, Africa, and South America (Fig. 1a), as

* Corresponding authors at: School of Earth Sciences, Yunnan University, Kunming 650500, China (Z. Zhao).
E-mail addresses: xiaojiafei@vip.gyig.ac.cn (J. Xiao), zhaozhifang@ynu.edu.cn (Z. Zhao).

https://doi.org/10.1016/j.oregeorev.2022.104813
Received 17 September 2021; Received in revised form 1 March 2022; Accepted 1 March 2022
Available online 4 March 2022

well as minor occurrences in many other parts of the world (Cook, 1992; Mi, 2010). Old phosphorite bearing strata that developed in South China (Fig. 1b) feature the preservation of a complete stratigraphic sequence, thus serving as ideal study subjects for elucidating phosphogenesis (Ye, 1989; Wu et al., 1999). The Ediacaran phosphorite is attractive to researchers because of the discovery of infaunal colonization (Xiao and Knoll, 1999; Yin et al., 2007; Zhou et al., 2007; Huldtgren et al., 2011; Igisu et al., 2014). In addition, the early Cambrian phosphorite, especially the Zhijin deposit, is well known for its high concentration of rare earth elements (REE) and Y (REE + Y) (Zhang et al., 2003; Zhang et al., 2004; Guo et al., 2017; Chen et al., 2019; Liu et al., 2020).

Several processes have been proposed for the formation of old phosphorite, including (1) in situ diagenetic mineralization driven by redox potential changes in pore water (Frohlich et al., 1983; Föllmi, 1996; Pufahl and Hiatt, 2012; Muscente et al., 2015), (2) reworking of previous phosphate deposits (Föllmi, 1996; Ilyin, 1998; Yang et al., 2019; Zhang et al., 2019), (3) abiogenic accretion (She et al., 2013; Yang et al., 2019), (4) hydrothermal precipitation (Guo et al., 2003; Shi, 2005; Deng et al., 2015), and (5) microbial breakdown of buried organic matter (Föllmi, 1996). In particular, diagenesis has been considered to have played a critical role in phosphogenesis (Shields and Stille, 2001; Chen et al., 2003; Muscente et al., 2015), during which the phosphate mineral phase transformed (Liu, 1989). Authigenic apatite phases, including octacalcium phosphate (OCP) and hydroxyapatite (HAP), which are thermodynamically unstable (Oxmann and Schwendenmann, 2014), would eventually transform into carbonate fluorapatite (CFA) along with the diagenetic process (Gunnars et al., 2004; Oxmann and Schwendenmann, 2014; Liao et al., 2019). Therefore, an OCP precursor mechanism has been hypothesized for apatite formation (Gunnars et al., 2004; Oxmann and Schwendenmann, 2014). This viewpoint is mainly based on the authigenic apatite physicochemistry of modern phosphate sediments (Oxmann and Schwendenmann, 2014), and the question whether this hypothesis holds true for long time-scale phosphogenesis remains uncertain.

Rare earth elements record associated environmental information and are widely used to study phosphogenesis processes(McArthur and Walsh, 1984; Elderfield and Sholkovitz, 1987; Bau et al., 1995; Holser, 1997; Ilyin, 1998; Shields and Stille, 2001; Emsbo et al., 2015; Deng et al., 2017). Generally, old phosphorites show typical enrichment of middle REEs (MREE) compared to light REEs (LREE) and heavy REEs (HREE), with small negative Ce and weakly positive Eu anomalies (Jarvis et al., 1994; Shields and Stille, 2001; Emsbo et al., 2015; Yang

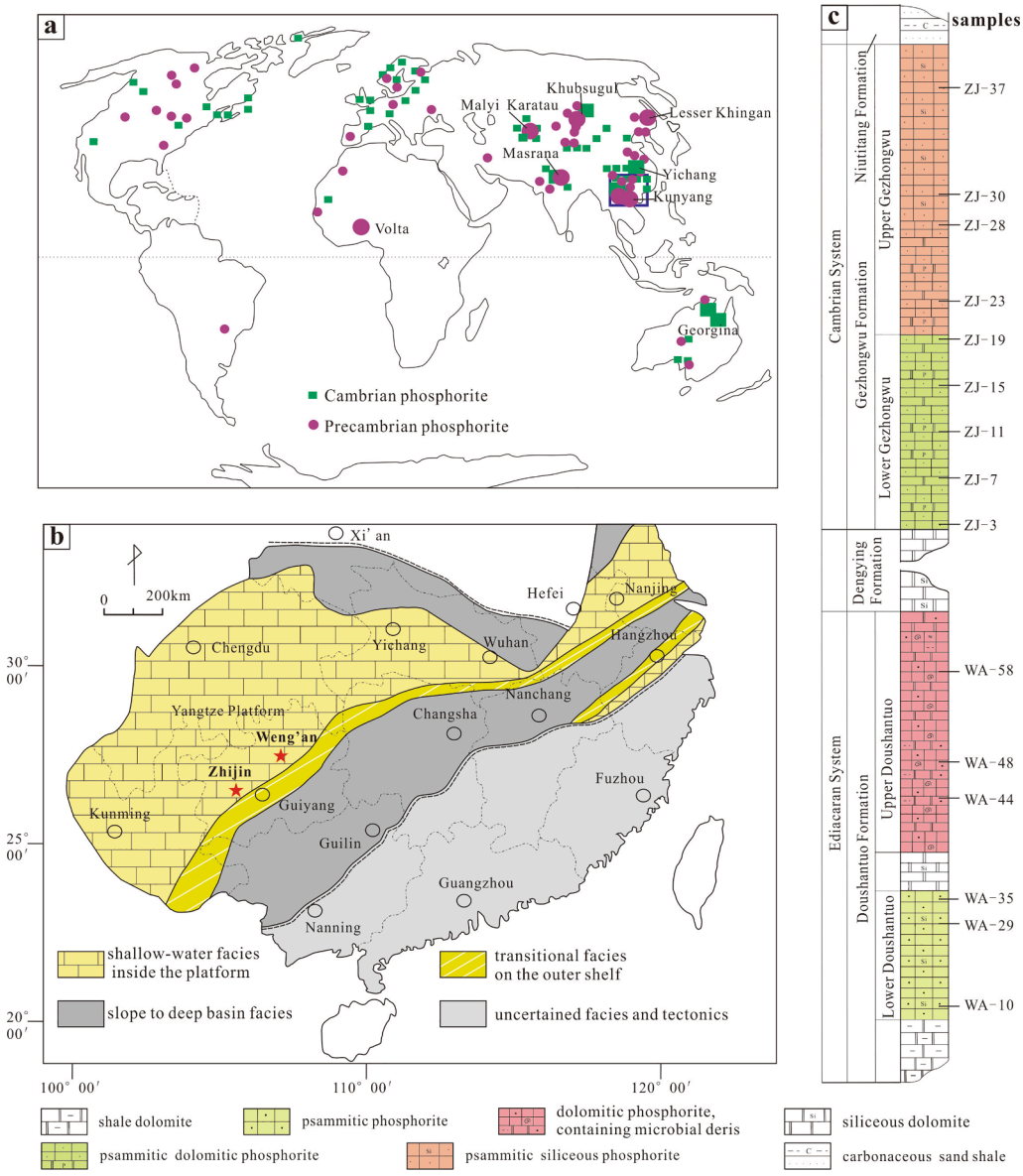

Fig. 1. (a) Distribution of Ediacaran to Cambrian phosphorite deposits, modified after Cook (1992) and Mi (2010). Smaller symbols represent minor deposits and occurrences, whereas larger symbols represent deposits with more than 100-million-ton phosphate rocks. (b) Simplified paleogeographic map of the Yangtze Platform in the Ediacaran-Cambrian Boundary, modified after Steiner et al. (2001) and Zhu et al. (2007). (c) Simplified and integrated stratigraphic columns and sampling locations of old phosphorite from South China. Ediacaran phosphorites were sampled from Weng'an deposit and the early Cambrian phosphorites from the Zhijin deposit.

et al., 2021a). On the other hand, REE + Y in Pliocene to Pleistocene and modern phosphate sediments (recent apatites) exhibit "seawater-like" shale-normalized (PAAS) patterns, with HREE enrichment and negative Ce anomalies (Emsbo et al., 2015; Liao et al., 2019; Lumiste et al., 2019). However, the REE + Y concentrations and distributions in recent sedimentary apatites are markedly discriminative in different fractions of apatitic grains (Liao et al., 2019; Lumiste et al., 2019), and similar characteristics were found in old phosphorite (Xin et al., 2015; Ye et al., 2020). This similarity has indicated that the REE + Y geochemical characteristics of apatite are prone to modification during diagenesis and are incapable of recording information on initial conditions (Trotter et al., 2016; Liao et al., 2019; Lumiste et al., 2019; Skinner et al., 2019). Nevertheless, it is worthwhile to clarify whether REE + Y record any initial depositional information after apatite alteration during diagenesis. This may shed light on another fundamental question in phosphorite research: can recent apatites be regarded as the incipient stage of old phosphorite? An important aspect of this question is the uncertainty of diagenetic differences and similarities between recent and long time-scale phosphogenesis.

Previous researchers have focused mainly on the bulk REE + Y characteristics of phosphorite. For the past few years, in situ analysis techniques have allowed micro-geochemical analysis of minerals, facilitating the tracing of origins, genesis, and formation conditions on a micro-scale. In this study, fine-scale mineralogical characteristics of apatites were analyzed using scanning electron microscopy (SEM), in situ major elements of phosphate minerals were analyzed using electron microprobe analysis (EMPA), and in situ trace elements were analyzed using laser ablation inductively coupled plasma mass spectrometry (LA-ICP-MS). With this new dataset, we aimed to determine the phosphogenesis and particularly the diagenesis of old phosphorite. Furthermore, the comparison of old apatites with recent apatites provides a holistic understanding of the formation of old phosphorite.

2. Background

2.1. Regional geology

The Ediacaran succession in South China was deposited on a passive continental margin on the Yangtze Platform (Jiang et al., 2007a; Jiang et al., 2011). Thereafter, the Cambrian stratigraphic sequence was sedimented during the unparalleled emergence of organisms (Steiner et al., 2001; Marshall, 2006; Zhu et al., 2007; Fox, 2016). From the late Ediacaran to the early Cambrian era, the facies regions of the Yangtze block were comprised of shallow-water facies carbonate platforms, transitional facies, and deep-water slope and basin facies from the northwest to southeast (Fig. 1b) (Steiner et al., 2001; Jiang et al., 2007a; Zhu et al., 2007). The lithofacies deposited in South China include continental, neritic, and abyssal clastic rocks, as well as deep sea siliceous rocks, along with the water deepening from the NW platform toward the SE ocean basin (Liu et al., 1993; Xue et al., 2001).

In the Central Guizhou, the Ediacaran and early Cambrian stratigraphic sequences developed completely. The Ediacaran successions in the sequence are represented by the Doushantuo Formation and the overlying Dengying Formation, whereas the early Cambrian successions are represented by the Gezhongwu Formation and overlying Niutitang Formation (Fig. 1c). The Ediacaran and early Cambrian phosphorite in the Central Guizhou, typically represented by the Weng'an and Zhijin deposits, is hosted in the Doushantuo and Gezhongwu formations, respectively (Fig. 1c). The Ediacaran phosphorite exposed in Weng'an county is underlain by Nantuo tillites and overlain by Dengying dolomite and is divided into lower and upper layers. The early Cambrian phosphorite exposed in Zhijin county is underlain by Dengying dolomite and overlain by Niutitang sandy shale and is also divided into lower and upper layers.

2.2. Deposit geology

2.2.1. Ore resources

The Weng'an deposit, divided into the Baiyan and Gaoping mining districts, had P resources reaching 0.794 billion tons and showed important economic and geological significance. The Zhijin phosphorite deposit, divided into Xinhua Mining and Damachang Mining districts, contains 3.39 billion tons of P ore resources, with REY resources (RE_2O_3) reaching 3.503 million tons with an average grade of 1036 g/t.

2.2.2. Stratum lithology

The Doushantuo Formation in Weng'an can be divided into four members, with lithologies as follows (Fig. 1c): (I) the bottom layer comprises dolomite with cross-bedding, horizontal bedding, and microscale wavy bedding; (II) Lower Doushantuo is a 10–50-cm thick ore body comprising off-white siliceous phosphorite, with parallel and horizontal bedding; (III) the interlayer comprises dolomite, siliceous dolomite, and chert; (Ⅳ) Upper Doushantuo is a ~30–60-cm thick ore body consisting of dolomitic phosphorite and abundant microbial debris, which have been identified as algae (Xiao et al., 1998; Igisu et al., 2014), animal embryos (Xiao et al., 1998; Yin et al., 2007; Igisu et al., 2014), acritarchs (Zhou et al., 2007; Muscente et al., 2015), and encysting protists (Huldtgren et al., 2011).

The Gezhongwu Formation of the Zhijin is divided into two members, with lithologies as follows (Fig. 1c): (I) Lower Gezhongwu is composed of dolomitic phosphorites, with parallel and cross-bedding; (II) Upper Gezhongwu comprises striped siliceous phosphorite with wavy bedding. Representative biological fossils of the Cambrian explosion are abundant in Zhijin deposit, such as small shell fossils (SSF), macroscopic bacterial colonies, arthropods, sponges, and zooplankton (Steiner et al., 2001; Fox, 2016; Cai et al., 2019).

2.2.3. Mineralogy

Principally, two distinctive types of sedimentary phosphate grains of the old phosphorite can be distinguished based on their morphology, namely authigenic grains (Fig. 2) and biodetritus (Fig. 3). Authigenic grains are characterized by round, elliptical, spindly structures, and coated grains with 200–300 μm in diameter and abundant quartz inclusions (Fig. 2b, e and h). Partial authigenic grains have developed isopachous shells and have even developed an oolitic structure (Fig. 2e), with the isopachous shells showing obvious growth striation (Fig. 2f). K-feldspar is found to accumulate together with apatites (Fig. 2i). Authigenic grains comprising closely accumulated apatite nanocrystals (Fig. 2c, f and i), were mainly found in the Lower Doushantuo and the Gezhongwu Formation. Authigenic apatites in Doushantuo and Gezhongwu formations both have spherulitic texture, with diameter of 20–200 nm.

The biodetritus (Fig. 3a, d, g and j) developed in both the Upper Doushantuo (Ediacaran) and entire Gezhongwu Formation (early Cambrian). The biodetritus in the Ediacaran, including embryos (Fig. 3b) and metazoan algae (Fig. 3e), have diameters ranging from 200 μm to 2 mm. Both algae and embryos are made up of oriented apatites with a hexagonal short-column shape and particle size of 100 nm*200 nm to 100 nm*500 nm (Fig. 3c and f). The biodetritus in the early Cambrian are mainly small shelly fossils (SSF), with a diameter of 100–300 μm (Fig. 3h and k), comprising spherulitic apatites of 20–50 nm in diameter (Fig. 3I and l). More proof distinguishing the phosphate grains and discussion of the formation mechanisms can be seen in our previous research (Yang et al., 2021a; Yang et al., 2021b).

3. Sampling and analytical methods

The Ediacaran samples were obtained from the Shangdatang profiles of the Weng'an phosphorite deposits (Fig. 1b, 27°1′57″ N and 107°23′47″ E), and the Cambrian samples from Motianchong drill hole 2604 in the Zhijin phosphorite deposits (Fig. 1b, 26°40′24″ N and

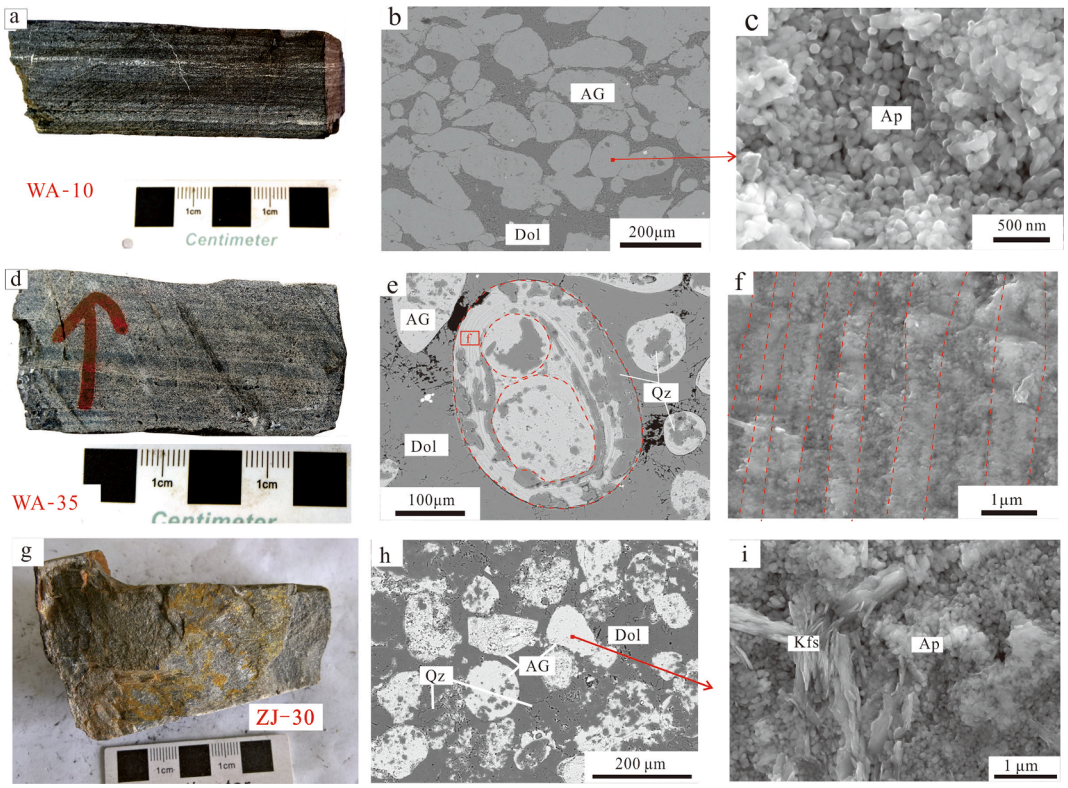

Fig. 2. Characteristics of the authigenic phosphorite specimens and SEM images of authigenic apatites from old phosphorite, South China. (a, d, g) authigenic phosphorite specimens show stripped structure; (b) granular authigenic grains comprise closely accumulated apatite nano-crystals (c); (e) oolitic grains have isopachous shells, representing obvious growth striation (f); (g) coated grains include abundant quartz inclusions and K-feldspar (i). Abbreviations: WA = samples from the Weng'an Ediacaran phosphorite deposit (a-f); ZJ = samples from the Zhijin early Cambrian phosphorite deposit (g-i); BG = biodetritus grain; AG = authigenic grain; Dol = dolomite; Qz = quartz; Ap = apatite; Kfs = K-feldspar.

105°51′30″ E). All the samples were sequential. The samples were made into polished sections with thickness of 50 μm for petrographic and in situ geochemical analyses, including major element compositions through EMPA and trace elements through LA-ICP-MS. The analytical methods are described in detail below.

3.1. Petrographic analyses

The petrographic characteristics were analyzed employing a JSM-7800F field emission SEM (Jeol Ltd., Japan) at the State Key Laboratory of Ore Deposit Geochemistry of the Institute of Geochemistry, Chinese Academy of Sciences. The beam emitted by the electric gun was turned into a high-energy electric beam by 10–30 kV acceleration voltage and, subsequently focused as a 1 μm microbeam to bombard the surface of the minerals. The backscattered electron images were collected with a 10 kV, 4.5 mA beam, and secondary electron images were collected with a 20 kV, 4.5 mA beam.

3.2. In situ major element analysis

In situ major elements of Ediacaran apatite were analyzed at the same State Key Laboratory of Ore Deposit Geochemistry employing a JXA8530F-plus instrument (Japan Electron Optics Laboratory [JEOL]). The high-pressure beam emitted by the electric gun was accelerated under 25 kV voltage and 10 mA current and bombarded the surface of the mineral, exciting characteristic X-rays. Subsequently, the X-ray signals were collected to analyze major elements. We used an apatite as standard. The detection limit was 0.01 % and the analytical error was less than 1 %. While in situ major elements of Cambrian apatite were analyzed in the EMPA Laboratory of the School of Earth Science, Zhejiang University, using a SHIMADZU 1720 H microprobe (Shimadzu Corporation, Japan). An accelerating voltage of 20 kV and current of 100 nA are required for the high-pressure beam to bombard the surface of the mineral, exciting characteristic X-rays. The ZAF (atomic number [Z], absorption effect [A], and fluorescence effect [F]) method was used for correction. Further, the mapping of the major elements (including P, Ca, and F) and partial REEs (including La, Ce, Pr, Nd, Gd, Yb, and Y) were conducted. For EMPA mapping analysis, 20 kV voltage, 100 nA current, and 40 ms/point were required. The analytical accuracy was 1–2 % and the detection limit 0.01 %.

3.3. In situ trace element analysis

In situ trace elements of apatite were analyzed at the State Key Laboratory of Ore Deposit Geochemistry of the Institute of Geochemistry, Chinese Academy of Sciences. The LA-ICP-MS instrument consists of a 193 nm Excimer Laser System (La) (Coherent Net-Solutions Pvt. Ltd., India) and Agilent 7700x (Agilent Technologies, Inc., USA) inductively coupled plasma mass spectrometer (ICP-MS). The samples were ablated by 44–60 μm laser beam and mixed with a gas carrier composed of H_2 and He_2, after which the aerosol was sent into the ICP-MS for element signal collection. Every signal collection cycle included 30 s blank and 50 s sample ablated signals. All elemental abundances were calibrated using NIST612 and NIST610 materials issued by the US National Institute of Standards and Technology (NIST) and using Durango apatite as apatite external standard. The internal corrections were applied using element abundances of Ca determined by EMPA analyses to correct matrix effects between the standards and the analyzed minerals. The signal was processed with LA-ICP-MS Data Reduction Software (ICPMCDataCal) developed by Liu et al. (2008) using a multiple external standard-internal standard method (Chew et al., 2016). The reference element contents of external standards are

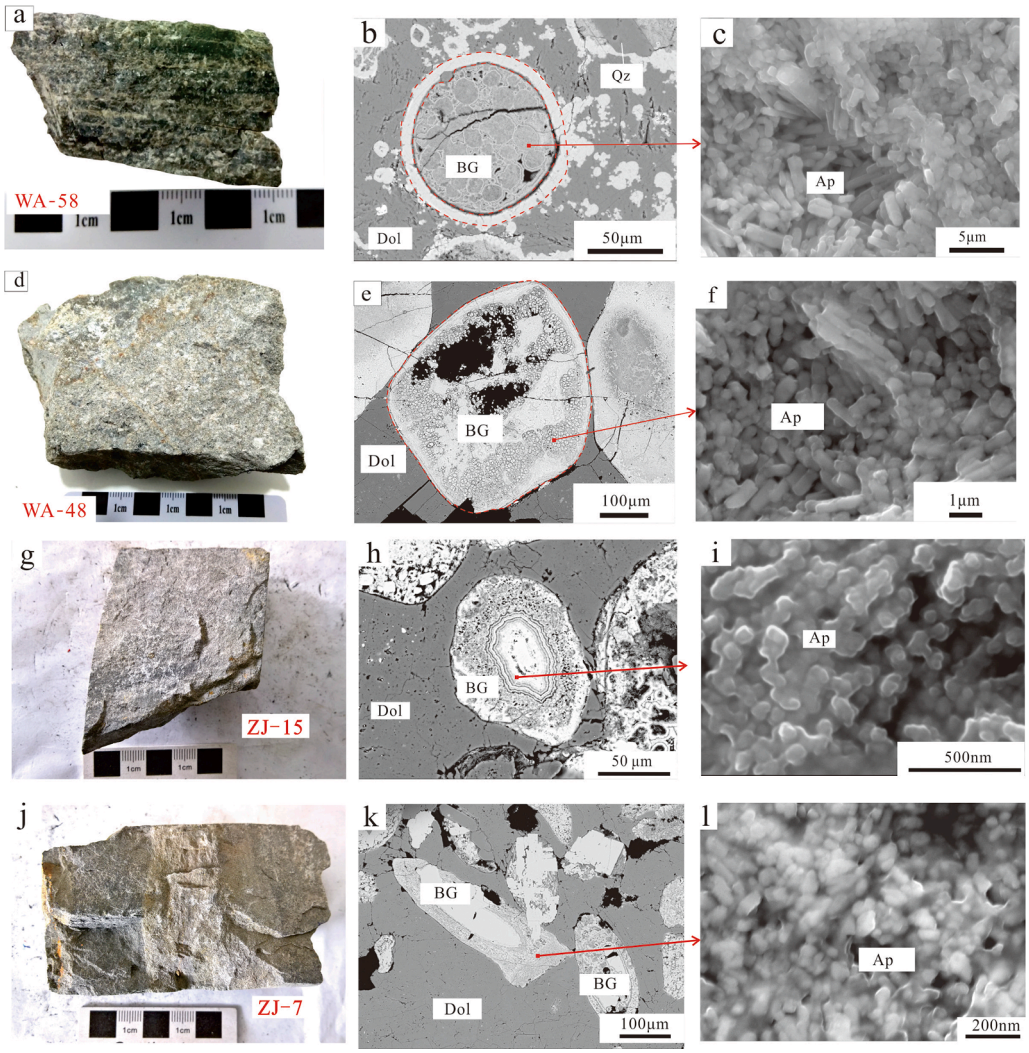

Fig. 3. Characteristics of biodetritus phosphorite specimens and SEM images of apatites from old phosphorite, South China. (a, d, g, j) biodetritus phosphorite specimens show massive and stripped structures; (b) embryos and (e) metazoan algae in the Upper Doushantuo, Ediacaran, made up of oriented six-party short-column apatite nano-crystals (c, f), respectively; (h, k) SSF in the Gezhongwu Formation, early Cambrian, comprising spherulitic apatite nano-crystals (i, l). Abbreviations: WA = samples from the Weng'an Ediacaran phosphorite deposit (a-f); ZJ = samples from the Zhijin early Cambrian phosphorite deposit (g-l); BG = biodetritus grain; AG = authigenic grain; Dol = dolomite; Qz = quartz; Ap = apatite; Kfs = K-feldspar.

available online at https://georem.mpch-mainz.gwdg.de/. Relevant diagnostic parameters were calculated according to the equations:

$Eu/Eu^* = 2Eu_N/(Sm_N + Gd_N)$ (Bau and Dulski, 1996); $Ce/Ce^* = 2Ce_N/(La_N + Nd_N)$ (Bau and Dulski, 1996); $Gd/Gd^* = Gd_N/(0.33Sm_N + 0.67Tb_N)$ (Bau and Dulski, 1996); $Y/Y^* = 2Y_N/(Dy_N + Ho_N)$(Shields and Stille, 2001); $Ce_{anom} = Lg(3*Ce_N/(2*La_N + Nd_N)$ (McLennan, 1989).

In these equations, "$_N$" represents the normalization against the Post-Archean Australian Shale (PAAS) standard (Taylor and McLennan, 1985).

4. Results

4.1. EMPA mapping of apatites

Authigenic grain (Fig. 4) and biodetritus (Fig. 5) from the Ediacaran and authigenic grain (Fig. 6) and biodetritus (Fig. 7) from the early Cambrian were selected for element mapping. The element distribution maps for F, P, Ca, La, Ce, Nd, Gd, and Y show that REE + Y are much higher in the outer rim of the grains than in the inner part in the biodetritus (Figs. 5 and 7), while the authigenic grains show relatively homogeneous REE + Y distributions (Figs. 4 and 6).

4.2. In situ major elements of apatites

The in situ major elements of Ediacaran and early Cambrian apatites are listed in Tables S1 and S2, respectively, and the significant numbers are listed in Table 1. The data showed inconspicuous differences between the Lower and Upper Doushantuos, with P_2O_5, F, and CaO values of 37.95–40.48 % (mean = 39.3 %, standard deviation (δ) = 0.51), 1.56–4.55 % (mean = 3.67%, δ = 0.41), and 47.11–55.23 % (mean = 53.77 %, δ = 0.39), respectively, in Ediacaran apatites. Likewise, the major elements of early Cambrian apatites also showed negligible difference between the Lower and Upper Gezhongwus, with P_2O_5, F, and CaO contents being 36.81–41.50 % (mean = 38.36 %, δ = 1.13), 1.48–3.77 % (mean = 3.00 %, δ = 0.05), and 53.20–57.37 % (mean = 55.58 %, δ = 0.55), respectively.

4.3. In situ trace elements of apatites

The in situ trace elements of Ediacaran and Cambrian apatites are listed in Tables S3 and S4, and the significant numbers of major elements are listed in Tables 2 and 3, respectively. Both Ediacaran and early Cambrian apatites are rich in Sr and Ba. Furthermore, apatites from the Upper Gezhongwu are rich in Zn and Pb. ∑REE + Y in Ediacaran apatites are less variable in the Lower Doushantuo, with a mean of 240.46 ppm (78.12–413.69 ppm, δ = 81.08), whereas those in the Upper Doushantuo differ notably among different samples (δ = 149.80) with a mean of 177.02 ppm (28.55–599.24 ppm). The early Cambrian apatites from Zhijin have higher ∑REE + Y compared to the Ediacaran apatites, with mean ∑REE + Y of 1811.30 ppm (530.25–3067.82 ppm, δ = 530.25) in the Lower Gezhongwu and 1831.39 ppm (1354.33–2324.01 ppm, δ = 284.42) in the Upper Gezhongwu.

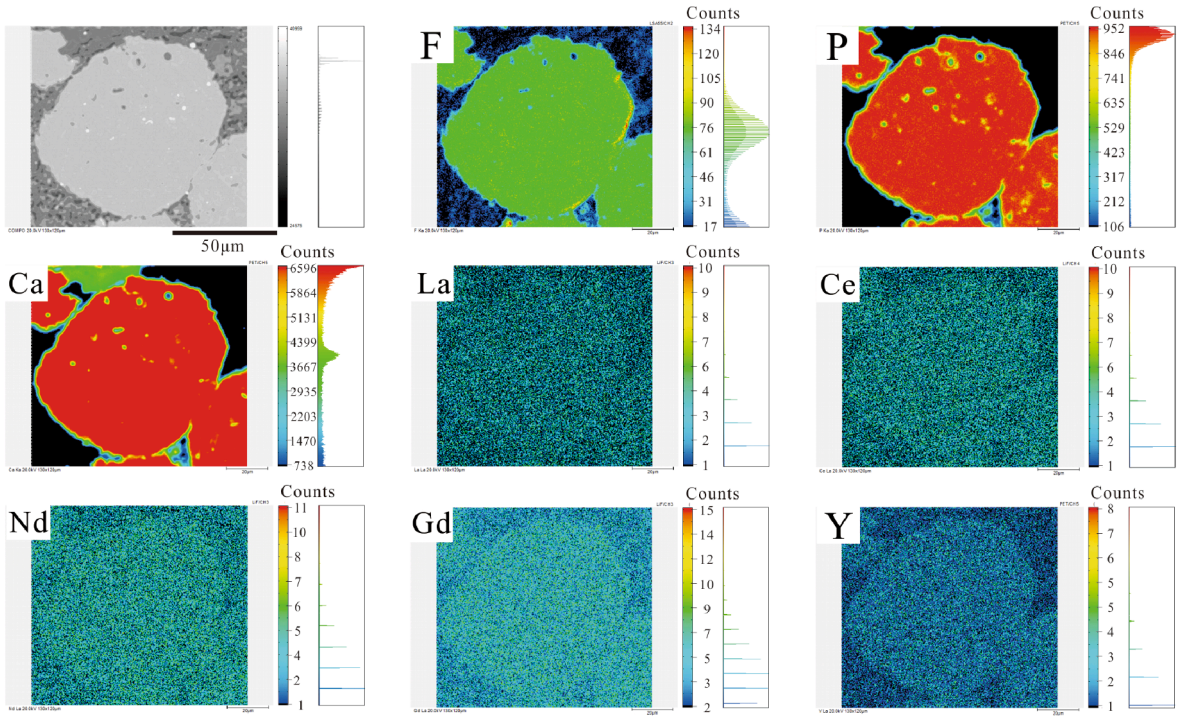

Fig. 4. EPMA mapping of major and partial REE + Y elements for authigenic grain from the Doushantuo Formation, Ediacaran in the Weng'an deposit, Central Guizhou. The signal acquisition conditions were: 20 kV voltage, 100nA current, and acquisition speed of 40 ms/point. The same conditions are true for Figs. 5-7.

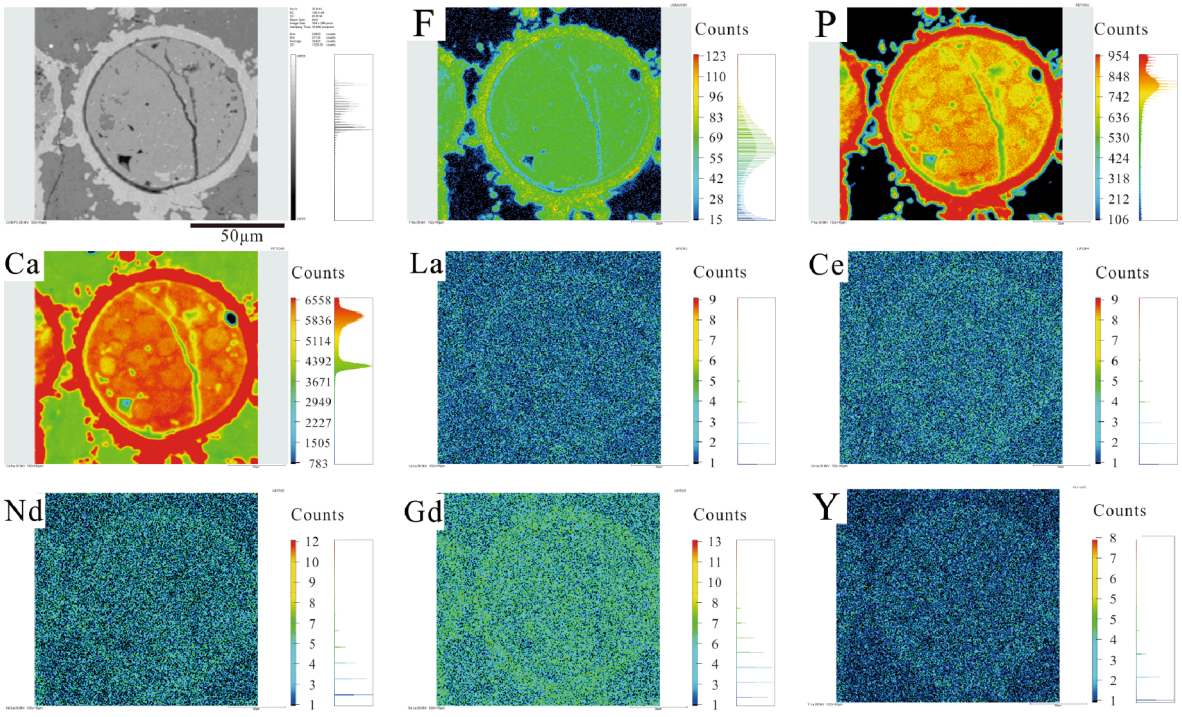

Fig. 5. EPMA mapping of major and REE + Y elements for biodetritus from Doushantuo Formation, Ediacaran in the Weng'an deposit, Central Guizhou.

Average Y/Ho ratios in Ediacaran apatites are 40.45 ($\delta = 2{,}51$), and those in Cambrian apatites are 52.13 ($\delta = 2.81$). No Eu anomalies were observed in the apatites, with much higher Eu/Eu* in the Ediacaran apatites (range 0.78–1.22, 0.99 on average) and constant Eu/Eu* values in the early Cambrian samples (range 0.83–1.05, 0.93 on average). Ce/Ce* values show a systematic decrease from the Lower Doushantuo (0.84–0.96, mean of 0.90 and δ of 0.03) to the Upper Doushantuo (0.54–0.72, mean of 0.63 and δ of 0.05), whereas those in Cambrian apatites are lower and less variable (0.30–0.44, with mean of 0.34 and δ of 0.03) (Fig. 8). In the Ce/Ce* vs Pr/Pr* plot, the Lower Doushantuo apatites showed no Ce anomalies, the Upper Doushantuo apatites exhibit unrealistic negative Ce anomalies, and apatites from the early Cambrian exhibit realistic negative Ce anomalies (Fig. 8). Most Ce_{anom} of Lower Doushantuo apatites >-0.1, ranging from -0.06 to -0.12,

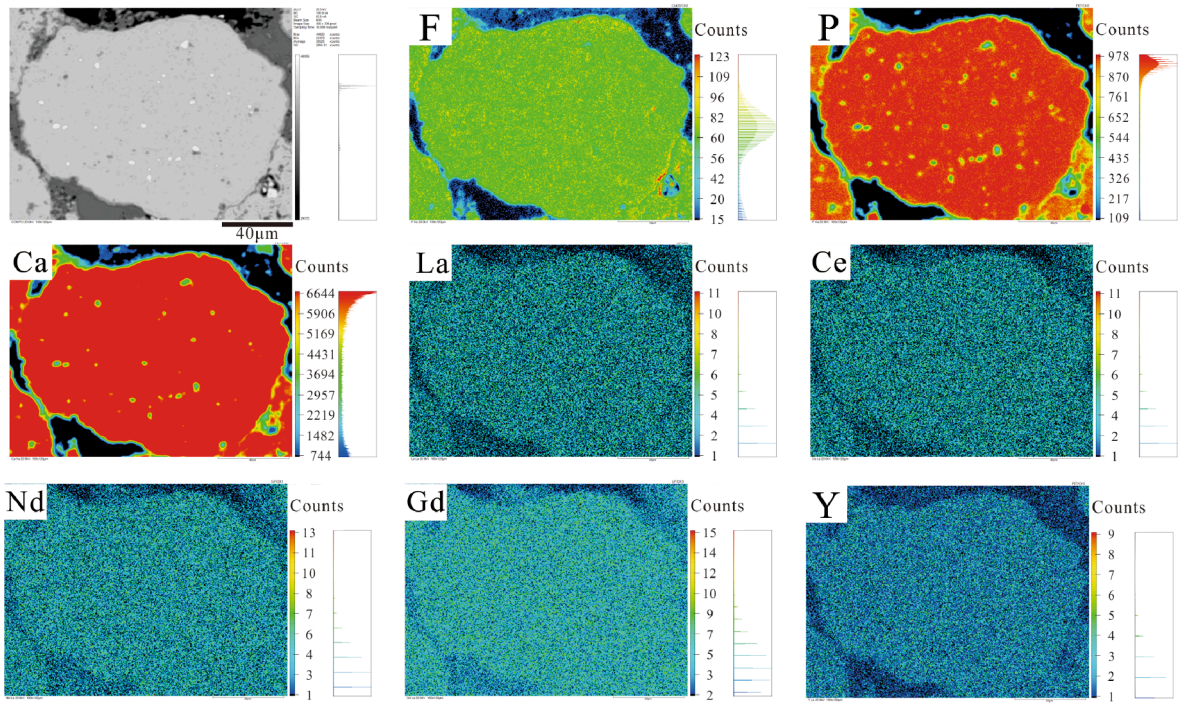

Fig. 6. EPMA mapping of major and REE + Y elements for authigenic grain from Gezhongwu Formation, early Cambrian in the Zhijin deposit, Central Guizhou.

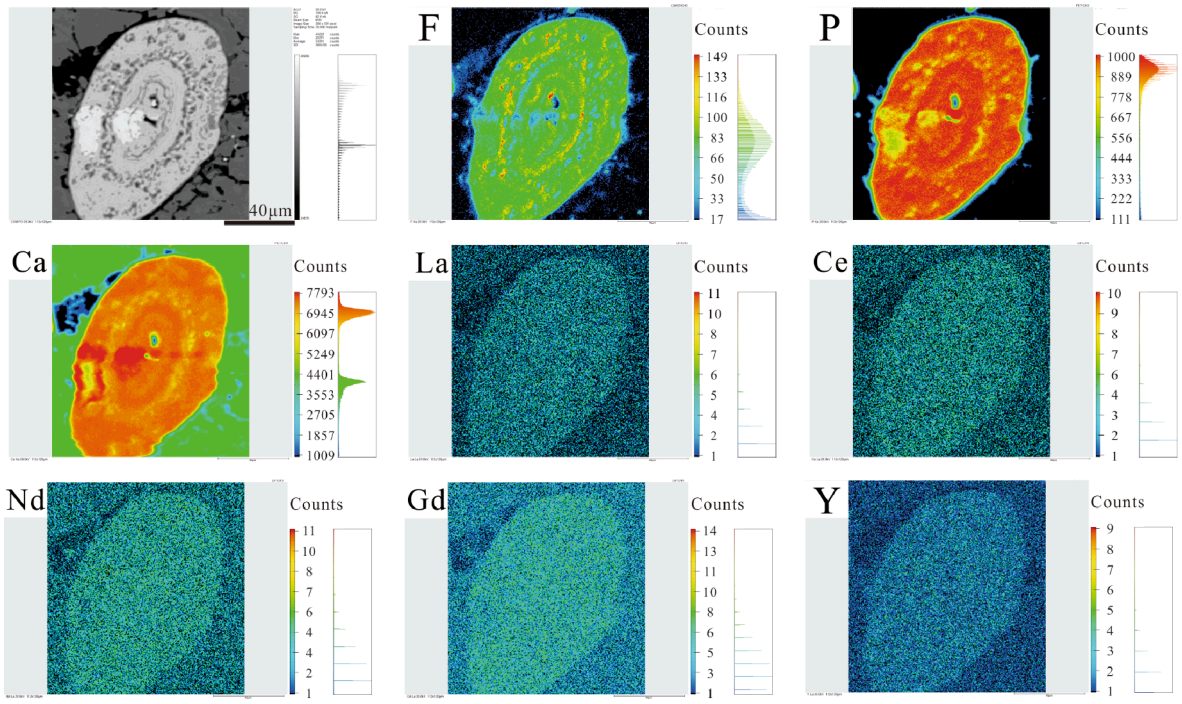

Fig. 7. EPMA mapping of major and REE + Y elements for biodetritus from Gezhongwu Formation, early Cambrian in the Zhijin deposit, Central Guizhou.

whereas all apatites from Upper Doushantuo and the early Cambrian are less than −0.1, with averages of −0.26 and −0.50, respectively. Y/Y*, Gd/Gd*, La_N/Sm_N, La_N/Nd_N, and La_N/Yb_N increase from Ediacaran to early Cambrian apatites (Tables 2 and 3). In plots between Ce/Ce* and Eu/Eu*, Y/Ho, Gd/Gd*, and Y/Y*, the data for apatites are relatively isolated from each other (Fig. 9). Generally, Ce/Ce* shows no correlation with Eu/Eu* (Fig. 9a) but shows negative relationships with Y/Ho (Fig. 9b), Gd/Gd* (Fig. 9c), and Y/Y* (Fig. 9d).

PAAS-normalized REE + Y patterns of old apatites can be divided into three types, namely (1) left-inclined types (Fig. 10a) found in the apatites from Lower Doushantuo, Ediacaran, which are characterized by depletion of LREEs, enrichment of HREEs, with Y/Ho ratios (38.36–43.34) lower than that of modern seawater (44–74) (Zhang et al., 1994), weakly positive La, Gd, and Y anomalies, and no Ce anomalies; (2) Shale-like patterns (Fig. 10b) found in the apatites from the Upper Doushantuo, Ediacaran, characterized by weak enrichment of MREE in comparison with LREEs and HREEs, with lower Y/Ho ratios (37.05–42.29), slightly negative Ce anomalies, and moderately positive

Table 1
Mean and extreme values of in situ major elements of Ediacaran and early Cambrian apatites from the Central Guizhou, South China (wt.%).

Stratum		CaO	Ca	FeO	SiO_2	P_2O_5	P	F	Y_2O_3	La_2O_3
Upper Doushantuo N = 66	Max	54.82	39.16	0.15	0.15	40.48	17.67	4.55	0.00	0.03
	Min	52.87	37.77	0.01	0.00	37.95	16.57	1.56	0.00	0.00
	Median	53.73	38.38	0.01	0.00	39.83	17.39	3.39	0.00	0.00
	Mean	**53.76**	**38.40**	**0.01**	**0.00**	**39.73**	**17.35**	**3.52**	**0.00**	**0.01**
	δ	1.03	0.74	0.03	0.00	0.44	0.19	0.40	0.00	0.01
Lower Doushantuo N = 47	Max	55.23	39.45	0.18	0.00	40.30	17.60	4.36	0.00	0.05
	Min	47.11	33.65	0.00	0.00	38.01	16.60	3.00	0.00	0.00
	Median	53.65	38.32	0.07	0.00	39.13	17.09	3.89	0.00	0.00
	Mean	**53.78**	**38.41**	**0.07**	**0.00**	**39.24**	**17.13**	**3.88**	**0.00**	**0.01**
	δ	0.54	0.39	0.04	0.02	0.51	0.22	0.41	0.00	0.01
Upper Gezhongwu N = 27	Max	56.98	40.70	2.81	0.23	41.36	18.06	3.77	0.14	0.13
	Min	53.20	38.00	0.00	0.00	37.17	16.23	1.48	0.00	0.00
	Median	55.01	39.29	0.13	0.13	38.18	16.67	3.14	0.01	0.07
	Mean	**54.98**	**39.27**	**0.43**	**0.13**	**38.42**	**16.77**	**3.00**	**0.04**	**0.07**
	δ	0.89	0.63	0.68	0.06	1.00	0.43	0.47	0.05	0.04
Lower Gezhongwu N = 19	Max	57.37	40.98	0.23	0.27	41.50	18.12	3.50	0.18	0.15
	Min	55.29	39.49	0.00	0.00	36.81	16.07	2.66	0.00	0.00
	Median	56.43	40.30	0.06	0.16	38.00	16.59	3.04	0.04	0.04
	Mean	**56.45**	**40.32**	**0.06**	**0.16**	**38.28**	**16.71**	**3.00**	**0.04**	**0.05**
	δ	0.55	0.40	0.06	0.07	1.13	0.50	0.23	0.05	0.04

Note: Max means maximum value, Min means Minimum value, δ represents standard deviation.

La, Gd, and Y anomalies; (3) "Hat-shaped" patterns (Fig. 10c, d) found in the early Cambrian apatites, characterized by notable enrichment of MREEs and evident depletion of HREEs, with higher Y/Ho ratios (46.02–56.16), remarkable negative Ce anomalies, and positive La, Gd, and Y anomalies.

5. Discussion

5.1. Formation processes of old phosphorite

5.1.1. Ce anomalies

REEs exhibit highly coherent behaviors and, generally, trivalent ions under normal circumstances. In particular, Ce is a redox sensitive element. Under oxic marine environments, Ce^{3+} is oxidized into Ce^{4+}, during which insoluble CeO_2 forms and is removed from seawater via scavenging by Fe and Mn oxyhydroxides or by organic matter in suspension (McArthur and Walsh, 1984; Holser, 1997; Alibo and Nozaki, 1999; Pourret et al., 2008; Bau and Koschinsky, 2009). This process leads to the fractionation of Ce with other lanthanides and strongly negative Ce anomalies in coeval sediments, e.g apatite. In contrast, in suboxic or anoxic seawater, Ce is reduced and behaves similarly to other lanthanides, producing less-negative or no Ce anomalies (Holser, 1997; Pourret et al., 2008). The Ce_{anom} values of apatites have been used to represent the redox conditions of seawater, with values less (greater) than −0.1 reflecting oxic (anoxic) conditions (Wright et al., 1987). In our samples, the Ce_{anom} of the Lower Doushantuo apatites ranged from −0.06 to −0.12, whereas the mean Ce_{anom} of Upper Doushantuo apatites (−0.26) and early Cambrian apatites (−0.50) decreased gradually (Fig. 8). Hence, it can be concluded that seawater remained anoxic in the early Ediacaran, and became more oxic in the late Ediacaran, after which it was completely oxidized until the early Cambrian. This conclusion is consistent with the results of previous reports (Wu et al., 1999; Zhang et al., 2004; Wu et al., 2006; Wen et al., 2011; Fan et al., 2014; Fan et al., 2016; Yang et al., 2019).

Nevertheless, Ce anomalies may attributable to positive La anomalies. To exclude such anomalies, Bau and Dulski (1996) proposed a Ce/Ce* vs Pr/Pr* plot to determine whether Ce anomalies are exaggerated by the La effect. In this study, the Lower Doushantuo apatites did not exhibit any Ce anomaly, the Upper Doushantuo apatites exhibit unrealistic Ce anomalies exaggerated by the La effect, and the early Cambrian apatites presented realistic negative Ce anomalies (Fig. 8). The Ce anomalies of apatites presented similar values to those of previously reported phosphorite bulk rocks (Yang et al., 2021a) and cotemporaneous carbonates (Yang et al., 2021b), revealing that the apatites record information carriers of seawater characteristics and depositional conditions.

5.1.2. Eu anomalies

Europium exhibits geochemical behavior similar to that of other REEs under low temperature conditions (~25 °C). However, Eu^{3+} becomes predominant under high temperatures (>250 °C) and elevated pressures. Accordingly, the hydrothermal fluids and their sediments are usually characterized by distinct positive Eu anomalies (Fig. 11) (Olivarez and Owen, 1991; Bau and Dulski, 1999; Douville et al., 1999; Bau et al., 2010). Therefore, Eu anomalies could be used to constrain the hydrothermal flux in seawater, proportional to the moderately mixed temperature (25–250 °C) of hydrothermal fluids and seawater (Goldstein and Jacobsen, 1988; Olivarez and Owen, 1991). In this study, the apatites have Eu/Eu* values close to 1 (Tables 2 and 3), indicating the limited influence of hydrothermal activities during apatite formation.

Being redox sensitive, Eu is oxidized to trivalent (Eu^{3+}) in oxic environments and converts to bivalent (Eu^{2+}) in reducing environments (Holser, 1997). Previous studies have suggested that Eu^{3+} could transfer to Eu^{2+} only under extremely reducing conditions, introducing Eu^{2+} into phosphorites and generating positive Eu anomalies (Baar et al., 1985; Kidder et al., 2003; Yang et al., 2019). However, the Ce/Ce* values of most apatites indicate suboxic to oxic conditions during the formation of old phosphorite, implying that Eu anomalies might not be the result of redox conditions.

Diagenesis has been considered as another influencing factor on Eu anomalies. During diagenesis, oxygen is depleted rapidly because of the degradation of organic matter, and the resulting anoxic condition favors the conversion of Eu^{3+} to Eu^{2+}which enters the crystal lattices of phosphate or carbonate minerals (Martinez-Ruiz et al., 1999; Kidder et al., 2003). According to research on REE in modern porewater, the porewater in deep locations under the seawater-sediment interface has negative Ce and positive Eu anomalies (Fig. 11) (Deng et al., 2017). This was interpreted as preferential Eu release into porewater from sediments, after which Eu entered apatites (Kidder et al., 2003; Deng et al., 2017). Our data show no Eu anomalies in apatites (Fig. 10), indicating no preferential Eu incorporation into apatites under diagenetic conditions (Joosu et al., 2016). Compared with the Eu/Eu* of bulk rocks, the apatites have lower Eu/Eu* values, which is particularly significant in the Ediacaran phosphorite (Yang et al., 2019; Yang et al., 2021a). It can be speculated that the released Eu^{2+} in porewater must enter other mineral phases during early diagenetic processes, such as calcite crystal

Table 2
Mean and extreme values of in situ trace elements of Ediacarcan apatites from Weng'an, the Central Guizhou, South China (ppm).

Sample		V	Cr	Co	Ni	Cu	Zn	As	Rb	Sr	Zr	Nb	Ba	Pb	La	Ce	Pr	Nd	Sm	Eu
Upper Doushantuo N	Max	8.76	88.86	7.22	1.84	5.59	49.89	45.61	1.17	1427.83	12.10	0.27	544.80	5.79	83.64	103.03	18.90	92.78	20.41	4.72
= 34	Min	0.65	0.59	0.02	0.00	0.00	7.09	3.75	0.01	504.03	0.65	0.04	174.29	0.79	2.45	3.91	0.65	3.74	0.98	0.24
	Median	1.73	2.92	0.07	0.42	1.16	30.87	6.74	0.14	1058.95	2.90	0.07	343.51	2.69	14.99	20.31	3.67	18.79	4.70	1.05
	Mean	**2.28**	**6.51**	**0.30**	**0.52**	**1.37**	**29.65**	**7.93**	**0.27**	**1015.59**	**3.57**	**0.08**	**356.39**	**2.90**	**25.38**	**31.15**	**5.77**	**28.02**	**6.18**	**1.39**
	δ	1.60	14.85	1.22	0.44	0.93	13.12	6.88	0.31	283.23	2.34	0.04	95.00	1.35	24.85	28.57	5.46	25.91	5.10	1.11
Lower Doushantuo N	Max	69.61	16.59	36.50	70.79	10.57	54.50	57.92	12.08	1895.66	35.74	2.10	986.91	42.95	51.07	101.58	11.49	53.96	11.97	2.87
= 41	Min	2.67	0.37	0.01	0.00	0.19	1.45	1.98	0.28	720.38	7.03	0.10	205.16	0.58	10.29	17.91	1.91	9.57	2.07	0.49
	Median	8.40	3.20	0.58	0.91	1.55	3.47	7.00	2.89	1351.18	19.15	0.40	567.55	3.67	30.17	53.49	6.41	30.24	6.77	1.66
	Mean	**12.51**	**3.64**	**2.71**	**4.59**	**2.52**	**8.85**	**12.80**	**3.46**	**1249.82**	**20.40**	**0.52**	**540.76**	**6.65**	**29.14**	**53.12**	**6.29**	**29.80**	**6.55**	**1.62**
	δ	11.41	2.85	6.30	11.69	2.82	11.46	13.51	2.49	324.33	6.40	0.39	213.06	9.37	9.87	18.61	2.22	10.43	2.33	0.56

sample		Gd	Tb	Dy	Ho	Er	Tm	Yb	Lu	Y	REY	Y/Ho	La_N/Sm_N	La_N/NdN	La_N/Yb_N	Y/Y*	Ce/Ce*	Eu/Eu*	Gd/Gd*	Ceanom
Upper Doushantuo N	Max	25.19	3.55	21.87	4.76	12.01	1.45	7.49	0.96	198.50	599.24	44.82	0.76	0.86	1.19	1.59	0.72	1.11	1.46	−0.18
= 34	Min	1.28	0.21	1.29	0.30	0.74	0.09	0.52	0.07	11.66	28.55	35.35	0.29	0.50	0.28	1.29	0.54	0.78	1.03	−0.31
	Median	5.80	0.92	5.67	1.17	3.10	0.38	2.17	0.30	45.45	129.48	40.28	0.48	0.73	0.52	1.46	0.64	0.94	1.20	−0.25
	Mean	**7.41**	**1.05**	**6.47**	**1.38**	**3.57**	**0.44**	**2.42**	**0.32**	**56.06**	**177.02**	**40.35**	**0.52**	**0.71**	**0.62**	**1.45**	**0.63**	**0.96**	**1.22**	**−0.26**
	δ	5.87	0.79	4.76	1.02	2.59	0.31	1.63	0.21	42.91	149.80	2.26	0.13	0.10	0.29	0.08	0.05	0.07	0.09	0.03
Lower Doushantuo N	Max	13.97	2.11	14.16	3.38	9.72	1.36	8.63	1.17	138.00	413.69	53.71	0.91	0.99	0.59	1.82	0.96	1.22	1.32	−0.06
= 41	Min	2.07	0.31	2.42	0.50	1.84	0.25	1.51	0.22	26.15	78.12	35.95	0.48	0.64	0.31	1.37	0.84	0.92	0.92	−0.12
	Median	8.63	1.28	8.65	2.12	6.25	0.85	5.20	0.73	85.04	246.98	39.77	0.64	0.83	0.43	1.54	0.90	1.01	1.17	−0.09
	Mean	**8.17**	**1.26**	**8.47**	**2.03**	**5.95**	**0.82**	**5.03**	**0.71**	**81.50**	**240.46**	**40.50**	**0.66**	**0.83**	**0.44**	**1.54**	**0.90**	**1.02**	**1.18**	**−0.09**
	δ	2.85	0.44	2.94	0.71	2.04	0.28	1.74	0.24	27.40	81.08	2.76	0.08	0.08	0.07	0.08	0.03	0.06	0.07	0.01

Table 3
Mean and extreme values of in situ trace elements of early Cambrian apatites from Zhijing deposit, the Central Guizhou, South China (ppm).

sample		V	Cr	Co	Ni	Cu	Zn	As	Rb	Sr	Zr	Nb	Ba	Pb	La	Ce	Pr	Nd	Sm	Eu
Upper	Max	39.78	352.52	5.07	26.27	63.19	10117.97	246.88	106.86	1495.79	36.19	2.85	1273.45	797.92	520.37	328.32	75.91	351.12	64.84	15.83
Gezhongwu	Min	0.67	1.46	0.04	0.23	0.44	0.98	1.91	0.04	860.31	1.45	0.04	313.23	9.39	316.84	158.24	43.84	196.02	36.15	7.77
N = 24	Median	8.82	9.72	0.14	1.98	9.72	131.65	15.63	22.26	1112.07	11.06	0.45	750.67	65.04	400.25	281.15	60.58	275.84	53.30	12.23
	Mean	**11.30**	**26.83**	**0.49**	**4.23**	**12.66**	**760.11**	**39.13**	**28.00**	**1117.28**	**13.87**	**0.62**	**741.76**	**107.76**	**410.69**	**258.19**	**61.39**	**275.89**	**50.46**	**11.52**
	δ	10.39	70.28	1.04	5.74	12.92	2118.06	53.60	28.92	175.55	11.21	0.68	275.77	162.02	56.07	55.76	9.49	45.84	8.95	2.37
Upper	Max	20.90	68.21	0.41	4.76	41.79	62.66	41.47	9.18	1223.93	6.68	0.21	895.38	21.41	735.78	423.63	115.60	522.85	94.59	18.99
Gezhongwu	Min	0.21	0.70	0.02	0.07	0.14	0.23	1.08	0.04	522.55	0.69	0.02	61.56	1.35	235.96	140.24	40.30	186.59	34.31	7.58
N = 29	Median	1.33	1.97	0.05	0.47	2.58	1.38	3.71	0.41	923.91	2.69	0.07	426.35	4.38	390.48	200.12	53.80	237.45	44.66	9.91
	Mean	**3.02**	**7.11**	**0.09**	**0.73**	**5.44**	**7.37**	**6.73**	**1.12**	**931.14**	**2.99**	**0.08**	**453.08**	**6.25**	**423.15**	**230.45**	**62.77**	**279.32**	**50.17**	**10.85**
	δ	4.69	15.24	0.10	1.02	9.28	14.61	8.95	2.14	191.93	1.53	0.05	209.24	5.47	131.96	83.67	21.40	92.91	16.03	2.93

sample		Gd	Tb	Dy	Ho	Er	Tm	Yb	Lu	Y	REY	Y/Ho	La_N/Sm_N	La_N/NdN	La_N/Yb_N	Y/Y*	Ce/Ce*	Eu/Eu*	Gd/Gd*	Ce_{anom}
Upper	Max	76.83	10.78	68.12	14.64	36.81	4.27	20.69	2.79	733.45	2324.01	56.16	1.50	1.52	2.04	2.07	0.44	1.03	2.80	−0.38
Gezhongwu	Min	43.50	5.92	37.42	8.32	20.68	2.47	11.92	1.49	457.34	1354.33	46.02	0.96	1.07	1.65	1.63	0.30	0.89	2.57	−0.57
N = 24	Median	64.06	8.76	51.15	11.17	28.19	3.26	16.46	2.02	569.46	1757.48	50.51	1.20	1.25	1.87	1.84	0.37	0.93	2.67	−0.46
	Mean	**61.50**	**8.47**	**52.11**	**11.42**	**28.52**	**3.29**	**16.46**	**2.02**	**579.28**	**1831.19**	**51.06**	**1.21**	**1.26**	**1.85**	**1.86**	**0.36**	**0.94**	**2.67**	**−0.48**
	δ	10.71	1.51	9.41	2.01	4.80	0.51	2.54	0.33	85.45	284.32	3.15	0.13	0.11	0.13	0.12	0.05	0.04	0.06	0.06
Upper	Max	110.98	15.33	91.10	18.83	44.72	4.86	22.17	2.41	900.46	3067.82	55.88	1.44	1.45	2.70	2.03	0.35	1.05	2.73	−0.48
Gezhongwu	Min	42.89	5.78	36.19	7.82	19.04	2.06	9.81	1.13	399.11	1171.94	47.34	0.78	0.88	1.75	1.67	0.30	0.83	2.58	−0.56
N = 19	Median	53.94	7.25	44.57	9.77	24.42	2.86	14.81	1.83	534.45	1614.67	54.64	1.29	1.33	1.99	1.98	0.31	0.91	2.67	−0.54
	Mean	**60.32**	**8.24**	**50.48**	**10.93**	**27.03**	**3.05**	**15.06**	**1.81**	**577.68**	**1811.30**	**53.41**	**1.25**	**1.28**	**2.03**	**1.93**	**0.31**	**0.91**	**2.65**	**−0.53**
	δ	18.29	2.64	15.41	3.16	7.50	0.73	3.03	0.33	136.59	530.25	2.57	0.16	0.14	0.23	0.11	0.01	0.06	0.05	0.02

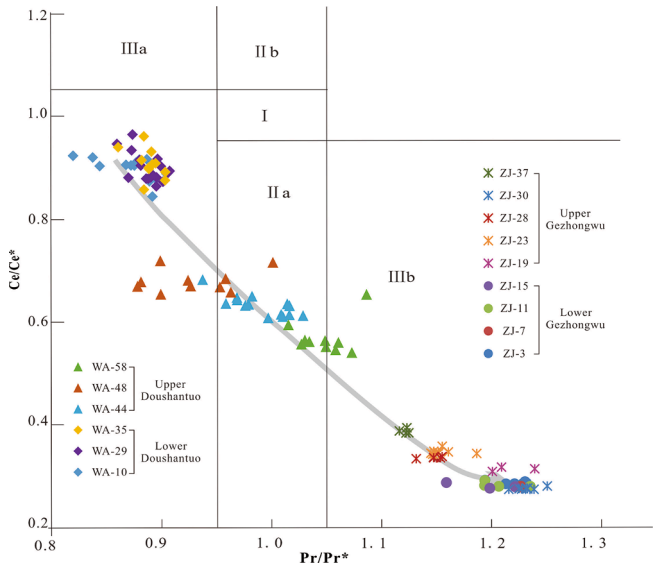

Fig. 8. Ce/Ce* vs Pr/Pr* plot. Field I: neither La nor Ce anomalies; Field IIa: unrealistic negative Ce anomaly due to positive La anomaly; field IIb: unrealistic positive Ce anomaly resulting from negative La anomaly; Field IIIa: true positive Ce anomaly; Field IIIb: true negative Ce anomaly. Modified after Bau and Dulski (1996). Diamonds and triangles represent apatites from Lower and Upper Doushantuo, respectively, with no Ce anomaly in Lower Doushantuo apatites and unrealistic Ce anomaly in Upper Doushantuo apatites. Dots and star-like shapes represent apatites from Lower and Upper Gezhongwu, respectively, with real negative Ce anomalies in all apatites. Ce/Ce* suggests anoxic conditions towards more oxic environments in the younger beds.

lattices (Trueman et al., 2003).

5.1.3. La, Gd, and Y anomalies

The fractionation among REE + Y usually occurs in seawater due to their solution complexation and surface complexation (partition coefficients, K^D) (Bau et al., 1996). Solution complexation increases with increasing atomic number, whereas surface complexation increases from La to Eu but decreases slightly from Eu to Yb, with La, Gd, and Y being exceptions (Bau et al., 1996). Further, Y has lower particle reactivity in natural waters, compared with other REEs (especially Dy and Ho) (Bau et al., 1996; Bau et al., 1997; Bau and Koschinsky, 2009). Therefore, in the presence of inorganic particles (e.g., hydrous Fe-Mn oxides) or organic matters, MREE are generally preferentially adsorbed, whereas La, Gd, and Y tend to remain in the seawater (Bau, 1996; Bau et al., 1996) and are recorded in the phosphorite. The Lower Doushantuo apatites have weakly positive La, Gd, and Y anomalies, whereas the apatites from Upper Doushantuo and the early Cambrian have increased positive La, Gd, and Y anomalies (Fig. 10). The positive correlations between Ce/Ce* and Gd/Gd* (Fig. 9c) and Y/Y* (Fig. 9d) plots show that the positive Gd and Y anomalies increased along with negative Ce anomalies (oxidized level) of seawater.

Yttrium and Ho, with similar charge and radius, always exhibit highly coherent behaviors and retain their chondritic ratios of 28 (Anders and Grevesse, 1989). Yttrium has stronger solution complexation than Ho in seawater (Byrne and Kim, 1990), and fractionation between Y and Ho thus occurs because Ho tends to be preferentially scavenged by Fe-Mn-oxyhydroxides/oxides or organic ligands (Bau et al., 1995; Bau et al., 1996; Bau et al., 1997). The negative relationships between Ce/Ce* and Y/Ho (Fig. 9b) suggest increased fractionation between Y and Ho with increasing level of oxidization in seawater. Further, fractionation between Y and Ho also occurred in sediments after precipitation (Bau, 1996; Lumiste et al., 2019), as shown by the clear decrease of Y/Ho ratios with continued diagenesis in recent

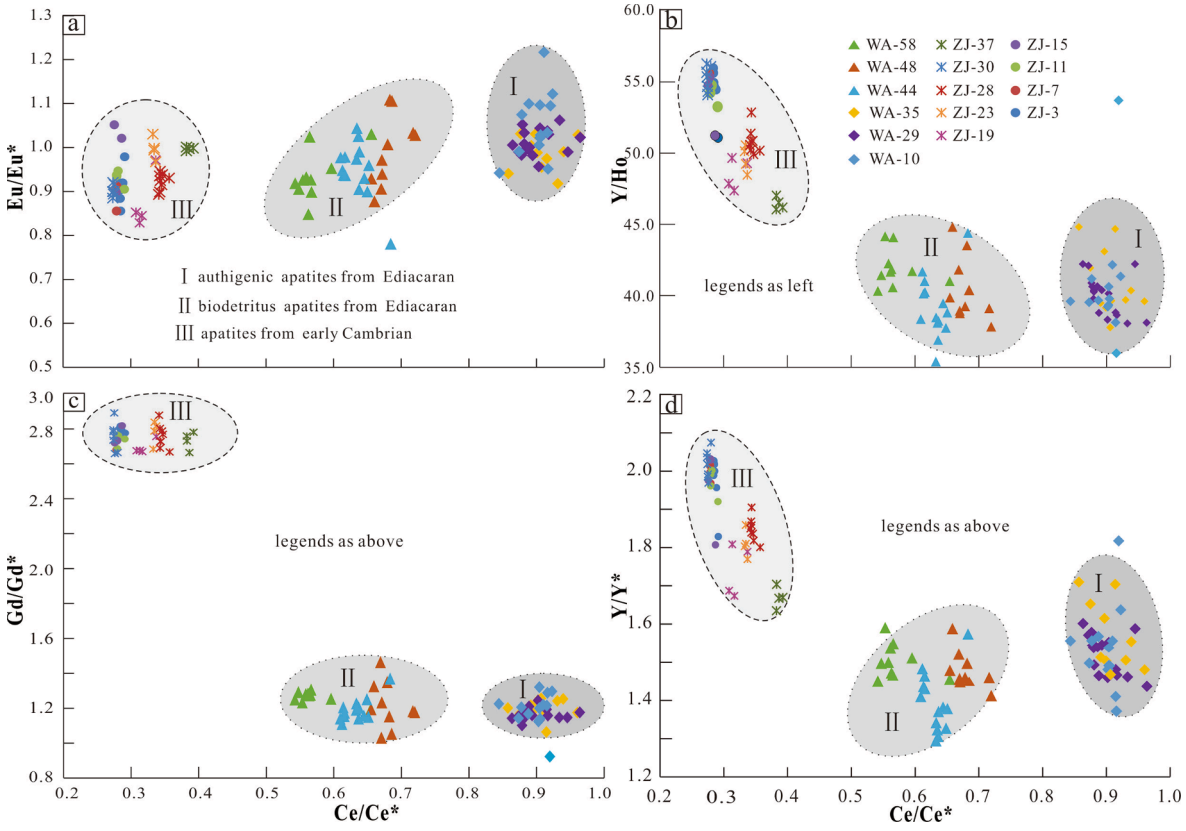

Fig. 9. Relationships between Ce/Ce* and Eu/Eu* (a), Y/Ho (b), Gd/Gd*(c), and Y/Y* (d) of old apatites in Central Guizhou, South China.

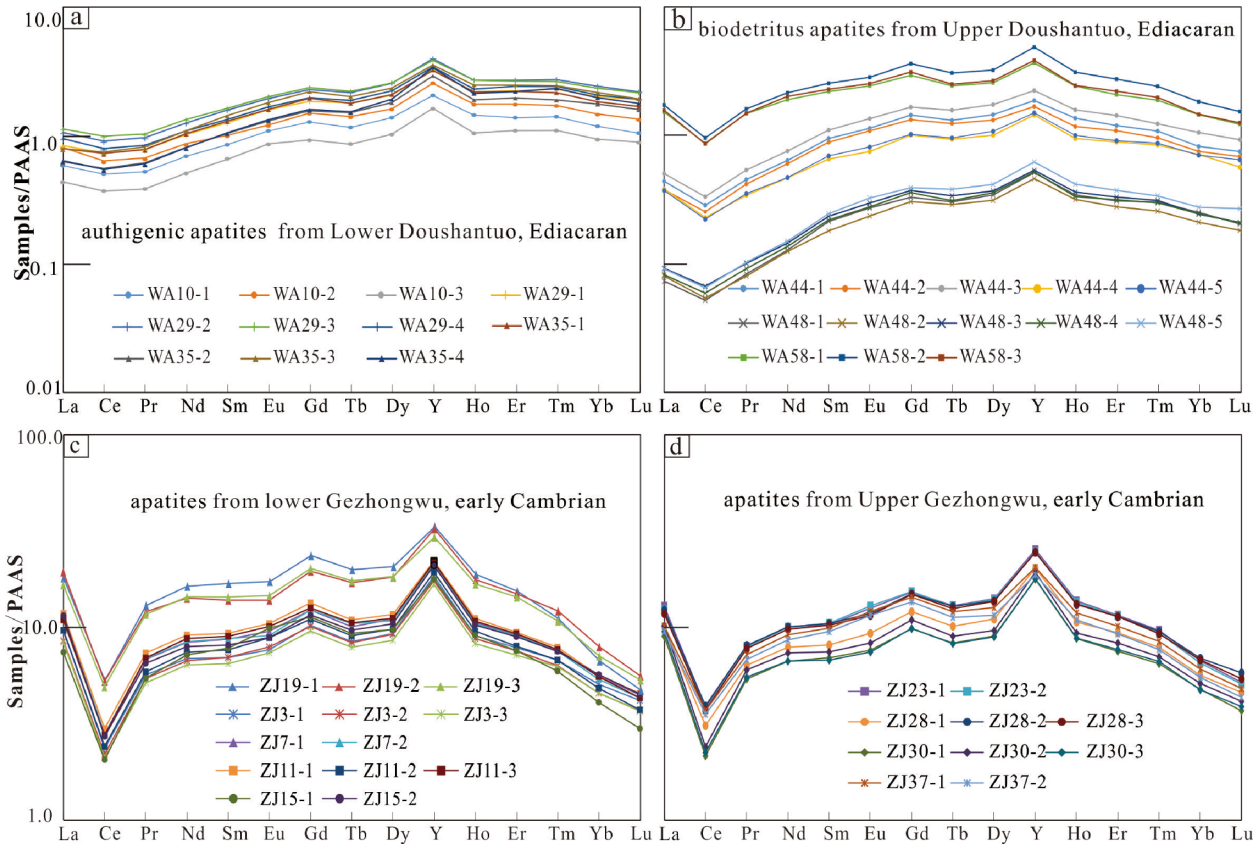

Fig. 10. PAAS-normalized REE + Y distributions of (a) authigenic and (b) biodetritus apatites from Doushantuo Formation, Ediacaran and apatites from Lower (c) and Upper Gezhongwus (d), early Cambrian (PAAS data from Taylor and McLennan (1985)).

apatites (Fig. 12) (Lumiste et al., 2019). In the Y/Ho vs Sm_N/Yd_N plot, old apatites, especially the Ediacaran apatites, were plotted in the diagenetic positions of recent apatites (Fig. 12), indicating the diagenesis of old apatites. However, the higher Y/Ho of early Cambrian apatites relative to the Ediacaran apatites is ascribed to the higher fractionation between Y and Ho of the early Cambrian apatites with higher level of oxidization.

5.1.4. *PAAS-normalized REE + Y patterns*

Seawater-like REE + Y patterns were ascribed to the initial signature of seawater, as REE + Y entered apatites directly, underwent limited diagenesis, or experienced limited exposure to REE enriched fluids (Elderfield and Pagett, 1986; Picard et al., 2002). Most phosphorite from the modern, Cenozoic, and Mesozoic eras exhibit such patterns (Grandjean et al., 1987; Jarvis et al., 1994; Lécuyer et al., 2004; Ounis et al., 2008; Kocsis et al., 2016). Researchers have suggested that deviations from the REE + Y patterns of modern seawater could be ascribed to diagenetic alteration (Elderfield and Pagett, 1986; Wright et al., 1987; Picard et al., 2002). Apatites preserving typical seawater patterns have lower ∑REE + Y, while those with higher ∑REE + Y are usually associated with "MREE-rich" patterns in phosphorite (Emsbo et al., 2015; Lumiste et al., 2021), which is controlled by the crystal-chemistry during diagenetic alteration (Reynard et al., 1999; Ounis et al., 2008). During diagenesis, REE + Y (especially MREE) adsorbed by oxyhydroxide particles and organic matter are released into pore water and redistributed among the authigenic phases (McArthur and Walsh, 1984; Ilyin, 1998; Shields and Stille, 2001; Bright et al., 2009; Chen et al., 2015; Deng et al., 2017). Ca-phosphates readily absorb MREE from porewater during diagenesis (Byrne et al., 1996) because of the high similarity of ionic radii between Ca and MREEs. As a result, porewater and sediments have higher MREE concentrations than seawater, producing MREE-rich apatites (Haley et al., 2004; Deng et al., 2017; Paul et al., 2019).

Lumiste et al. (2021) concluded that PAAS-normalized REE + Y patterns of sedimentary apatites could be divided into three groups, with gradually proceeding diagenesis: (1) seawater-like patterns, characterized by negative Ce anomalies with varying degrees of HREE enrichment (Shields and Stille, 2001; Emsbo et al., 2015); (2) shale-like patterns, characterized by small or absent Ce anomalies with little to no HREE enrichment (McArthur and Walsh, 1984; Lumiste et al., 2019); (3) "bell-shaped" MREE -enriched patterns with no Ce anomalies and depletion of LREE and HREE (Emsbo et al., 2015; Lumiste et al., 2021). In apatites, Ce anomalies diminish due to uptake of REE + Y from suboxic to anoxic porewater (Lumiste et al., 2021). However, Ce anomalies in the apatite of this study might provide information on seawater conditions (discussed in section 5.1.1). Under anoxic conditions during the early Doushantuo, limited REE + Y bounded by oxyhydroxide particles and organic matter were released into porewater; subsequently, apatites absorbed the limited REE + Y and recorded seawater patterns (Fig. 14a). Under suboxic to oxic seawater conditions, oxyhydroxide particles and organic matter carried MREE into porewater through preferential adsorption. Subsequently, MREE released by the dissolution of carrier phases were absorbed by recrystallized apatites, leading to REE + Y enrichment and MREE-rich patterns (Fig. 14b and c). Redox conditions of seawater could be responsible for the temporal variability of old phosphorite from South China, in which more oxic conditions result in more significant MREE enrichment (Fig. 10).

Weathering and leaching processes are considered another driver of element fractionation. As HREE have higher solution complexation compared to LREE, they were leached preferentially during weathering (McArthur and Walsh, 1984; Bau et al., 1995; Shields and Stille, 2001; Bright et al., 2009). In our samples, biodetritus exhibited HREE depletion (Fig. 10 b-d), similar to those of their phosphorite bulk rocks (Yang et al., 2019; Yang et al., 2021a), which might be a result of weathering

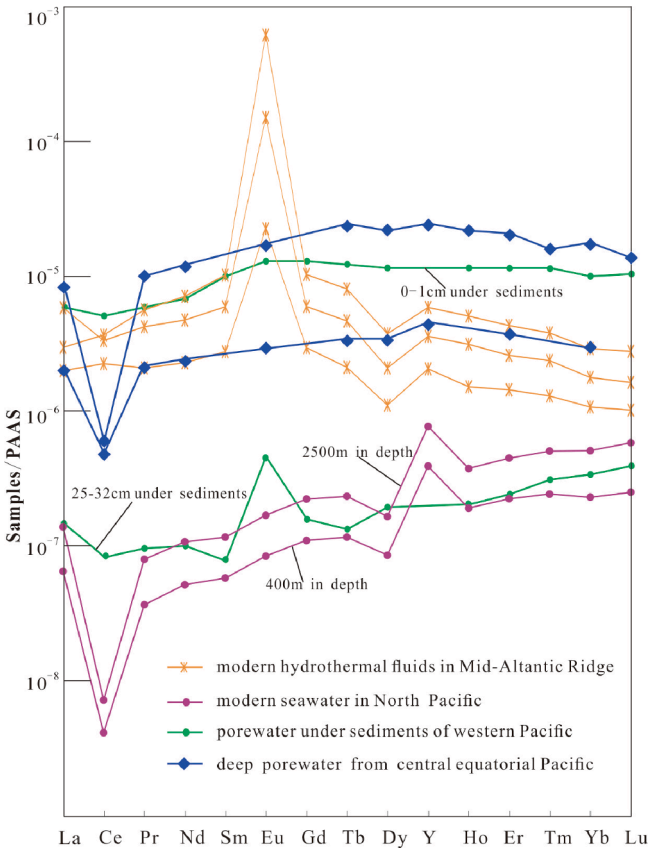

Fig. 11. PAAS-normalized REE + Y distributions of modern seawater, porewater, and hydrothermal fluids. PAAS data from Taylor and McLennan (1985); porewater data based on Deng et al. (2017); deep porewater data based on (Paul et al., 2019); modern seawater data based on Alibo and Nozaki (1999); modern hydrothermal fluid data based on Bau and Dulski (1999).

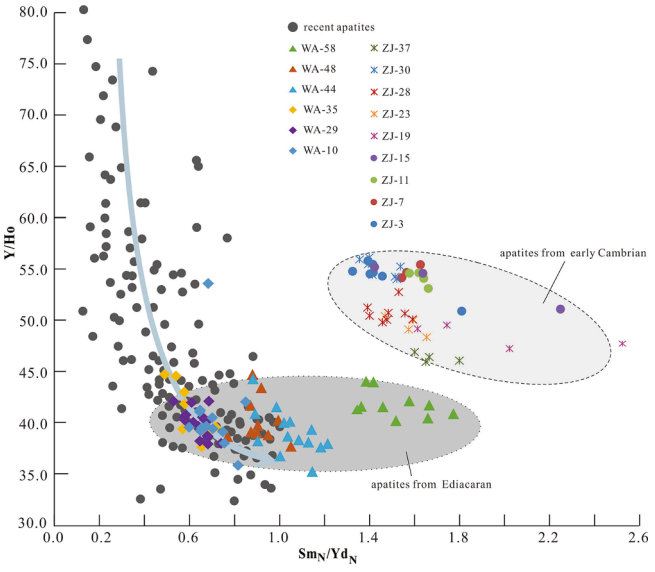

Fig. 12. Binary diagram of Y/Ho and Sm_N/Yd_N of the old apatites and recent apatitic grains. Apatites from the Ediacaran and the early Cambrian from this study, recent apatitic grains from the Namibian shelf of the Atlantic Ocean from Lumiste et al. (2019).

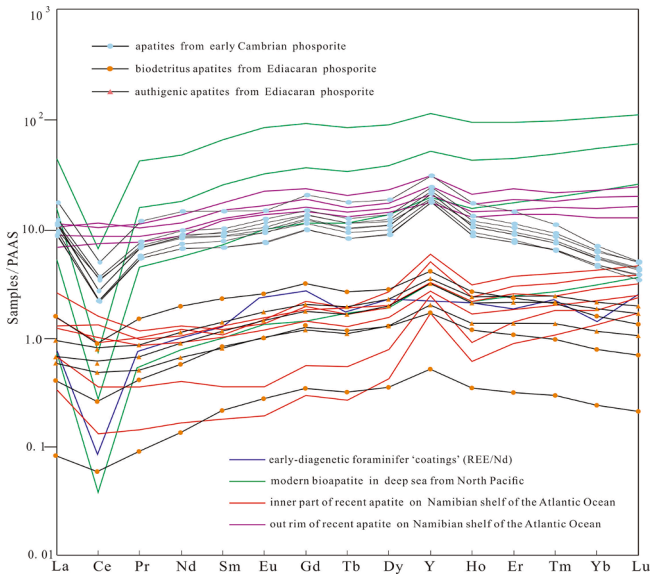

Fig. 13. PAAS-normalized REE + Y distribution patterns of old apatites and recent apatitic grains. PAAS data are based on Taylor and McLennan (1985)). Ediacaran and Cambrian apatites were analyzed in this study, and in situ REE + Y data are the mean values of each polished section. Other data: early-diagenetic foraminifera 'coatings' from Skinner et al. (2019), modern biogenic apatites in deep sea of the North Pacific from Liao et al. (2019), and recent apatites on the Namibian shelf of the Atlantic Ocean from Lumiste et al. (2019).

leaching (Yang et al., 2021b). However, authigenic apatites from the Ediacaran exhibited left-inclined REE + Y patterns (Fig. 10 a), similar to modern seawater (Fig. 11) besides except HREE depletion and no Ce anomalies, indicating minor weathering and diagenesis after deposition.

5.1.5. *REE + Y concentrations in phosphate grains*

According to bioapatite studies, uptake processes are thought to be relatively quick (<10^6 years) (Trueman and Tuross, 2002; Kohn, 2008). However, the early depositional signals maybe be altered by diagenetic processes, and REE concentrations might increase with continued diagenesis (Kocsis et al., 2010; Yang et al., 2021b). Previous analyses on spherical microfossils from the Ediacaran and nodules from the early Cambrian showed that REE concentrations that systematically increased from the core to rim occurred in phosphatized grains (Jiang et al., 2007b; Zhu and Jiang, 2017). This characteristic is attributed to diagenetic alteration, during which REE diffusion from the external environment (pore fluid) was expected to have enriched the rims more than the core, especially for originally large grains (Jiang et al., 2007b; Zhu and Jiang, 2017). The same characteristic was observed in biodetritus from the old phosphorite (Figs. 5 and 7), whereas ∑REE + Y variations were not prominent in authigenic grains (Figs. 4 and 6). The higher ∑REE + Y in the outer rim of biodetritus (Figs. 5 and 7) indicates that greater REE + Y uptake occurred in the outer parts than in the inner core during the diagenetic process (Fig. 14b, c). Our previous research showed that REE + Y enrichment of early Cambrian apatites was dominant by early diagenesis (Yang et al., 2021b). However, the relatively homogeneous REE + Y concentrations in the authigenic grains (Figs. 4 and 6) indicate that apatite recrystallization and REE + Y uptake might have occurred rapidly, following which the apatites were exposed to REE + Y-limited surroundings during diagenesis (Fig. 14a).

Precipitated phosphates in the water-sediment interface, including organic and inorganic P, were buried and subjected to diagenetic processes, and apatites finally formed (Liu, 1989; Ingall and Vancappellen, 1990; Ruttenberg and Berner, 1993; Yuan et al., 2019). The hypothesis proposed for the formation of modern apatite provides a fundamental interpretation for old apatites. The pathway of biogenic apatite

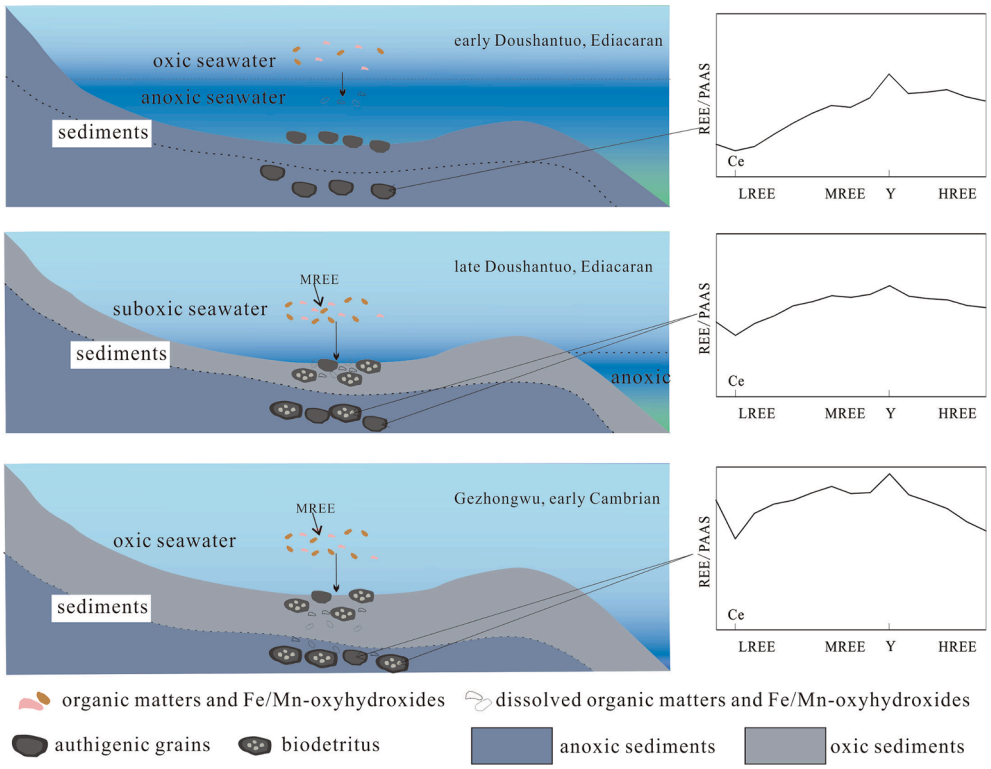

Fig. 14. Conceptual model of REE + Y uptake into old apatites under variable redox seawater conditions. (a) Under anoxic conditions, limited organic and Fe/Mn-oxyhydroxides existed in seawater, apatite recrystallization absorbed limited REE + Y; (b, c) Under suboxic to oxic seawater conditions, organic matters and Fe/Mn-oxyhydroxides carried MREES into porewater, subsequently, REEs were released due to the dissolution of carriers and then absorbed by recrystallized apatites. More oxic seawater conditions were associated with higher REE + Y enrichment and MREE-rich patterns. EDA: early diagenetic area; LDA: late diagenetic area.

regeneration is similar to that of modern sediments, which formed through enzyme-catalyzed hydrolysis of organic debris (Joshi et al., 2015; Yuan et al., 2019). During this process, buried organic P transformed to inorganic P, namely mineralization of P-containing organic matter (Ingall and Vancappellen, 1990; Ruttenberg and Berner, 1993; Yuan et al., 2019). Regardless of P sources, after mineralization, authigenic apatites underwent transformation during diagenesis. Thermodynamically unstable authigenic apatite phases, including OCP and HAP, have been reported in modern sediments (Oxmann et al., 2008; Oxmann and Schwendenmann, 2014), and these phases served as primary authigenic apatite phases. Oxmann and Schwendenmann (2014) studied different apatite phases and the solubilities of modern coastal sediments, suggesting that OCP served as the precursor of apatite formation and finally transformed into CFA with continued diagenesis (Gunnars et al., 2004; Oxmann and Schwendenmann, 2014; Liao et al., 2019). Even though CFA was the thermodynamically stable apatite phases in seawater (Jahnke, 1984; Knudsen and Gunter, 2002), CO_2 would be lost during the diagenetic process, leading to the formation of fluorapatite (FAP) (Liu, 1989). Old phosphorite comprises a vast majority of FAP and a small quantity of CFA, see Yang et al. (2021b), which strongly supports this process. Therefore, we propose that the apatites were readily recrystallized with continued diagenesis and diagenetic alteration over the course of a long geologic period. Biodetritus apatites have larger and more complete crystals (Fig. 3c, f, I and l) than authigenic apatites (Fig. 2c, f and i), indicating stronger diagenetic recrystallization of biodetritus. This suggests that authigenic apatites were relatively more stable than biodetritus during diagenesis, maintaining the initial REE + Y characteristics of seawater.

5.2. Comparative analyses of genetic processes

5.2.1. Comparisons with recent apatites

5.2.1.1. Similarities. Compared with in situ REE + Y compositions of old apatites, recent apatites have similar REE + Y concentrations and positive La, Gd, and Y anomalies (Fig. 13) (Liao et al., 2019; Lumiste et al., 2019). Furthermore, in Y/Ho vs Sm_N/Yd_N plot, old apatites were plotted in the diagenetic area of recent apatites (Fig. 12), illustrating further diagenetic modification of the old apatites. Researchers have shown that the ancient ocean had similar P fluxes, accumulation, and burial rates compared with the modern phosphate sediments from the Peru margin (Filippelli and Delaney, 1992; Filippelli, 2008). Therefore, if the initial REE + Y compositions of the ancient ocean resemble modern seawater, the similarities between old apatites and recent apatites indicate that recent apatites could serve as predecessors of old apatites, especially biodetritus.

5.2.1.2. Differences. Some studies suggested that the REE + Y compositions of ancient phosphorite deposits are dissimilar to modern phosphogenesis because of secular changes in oceanic conditions (Elderfield and Greaves, 1982; Shields and Stille, 2001; Emsbo et al., 2015). In reality, there are differences between old and recent apatites. Biodetritus apatites from old phosphorite have remarkable real negative Ce anomalies (Fig. 8), similar to modern bioapatites (Fig. 13) (Liao et al., 2019). However, authigenic apatites from the early Doushantuo have no Ce anomalies, consistent with the inner part of recent apatitic grains (Fig. 13) (Lumiste et al., 2019). These findings are ascribed mainly to the redox ocean conditions during apatite formation (Wu et al., 2006; Yang et al., 2019; Yang et al., 2021a). Moreover, another contributor to the alteration of Ce anomalies was diagenesis, during which Ce^{4+} was released into pore water and reduced to Ce^{3+} under reducing conditions (McArthur and Walsh, 1984; Shields and Stille, 2001; Bright et al., 2009; Chen et al., 2015). Trivalent Ce enters the structure of apatites, masking initial Ce anomalies and even causing positive Ce anomalies (Takahashi et al., 2015; Lumiste et al., 2019). This is reflected in the weaker negative Ce anomalies in pore water under sediments (Fig. 11) (Deng et al., 2017) and the absence of Ce anomalies in the outer rim of modern apatitic grains (Fig. 13) (Lumiste et al., 2019). Therefore, as Ce anomalies could be altered during the diagenetic process, other geochemical indexes should also be considered when using Ce anomalies as paleo-seawater redox proxies (Reynard et al., 1999; Shields and Stille, 2001).

Another significant characteristic is that the REE + Y patterns of

recent apatites are associated with HREE enrichment (Fig. 13), whereas those of old apatites are associated with HREE depletion. Furthermore, REE + Y compositions are significantly different between the outer rim and central parts in Cambrian phosphate nodules from South China (Jiang et al., 2007b). In the Ediacaran phosphorite, despite the lower ∑REE + Y, the PAAS-normalized patterns did not differ between the outer rim and inner part (Zhu and Jiang, 2017). This could simply be related to the grain size, in which smaller grains can incorporate REEs more easily with a rather homogenous distribution, masking the discrepancy between the outer rim and inner part. Recent apatites have higher ∑REE + Y in the outer rim than in the inner parts, with HREEs decreasing from the center to the rim, suggesting that diagenetic alteration occurred in the outer rim while the initial compositions were retained in the inner part(Lumiste et al., 2019). Both recent apatites and planktonic foraminifera surfaces correspond to the early stage of diagenesis (Liao et al., 2019; Lumiste et al., 2019; Skinner et al., 2019). Another cause is fractionation induced by uptake mechanism of diffusion from the external REE source (i.e., pore fluid, seawater, etc.) into the apatite structure (Cherniak, 2000; Kohn, 2008), resulting in relatively higher HREE content in the internal part than the external part (Trueman et al., 2011; Herwartz et al., 2013). Further, HREEs preferentially leach during weathering due to their high solution complexation compared with LREEs (McArthur and Walsh, 1984; Bau et al., 1995; Shields and Stille, 2001; Bright et al., 2009), accounting for another important aspect of HREE depletion in old apatites. Therefore, HREE depletion in old apatites illustrates longer diagenesis and weathering, and recent apatites might represent the early diagenetic stage, providing further understanding for the diagenesis of old apatites.

5.2.2. *Comparisons of old phosphorite around the world*

5.2.2.1. Comparisons of REE + Y compositions. Old phosphorites occur

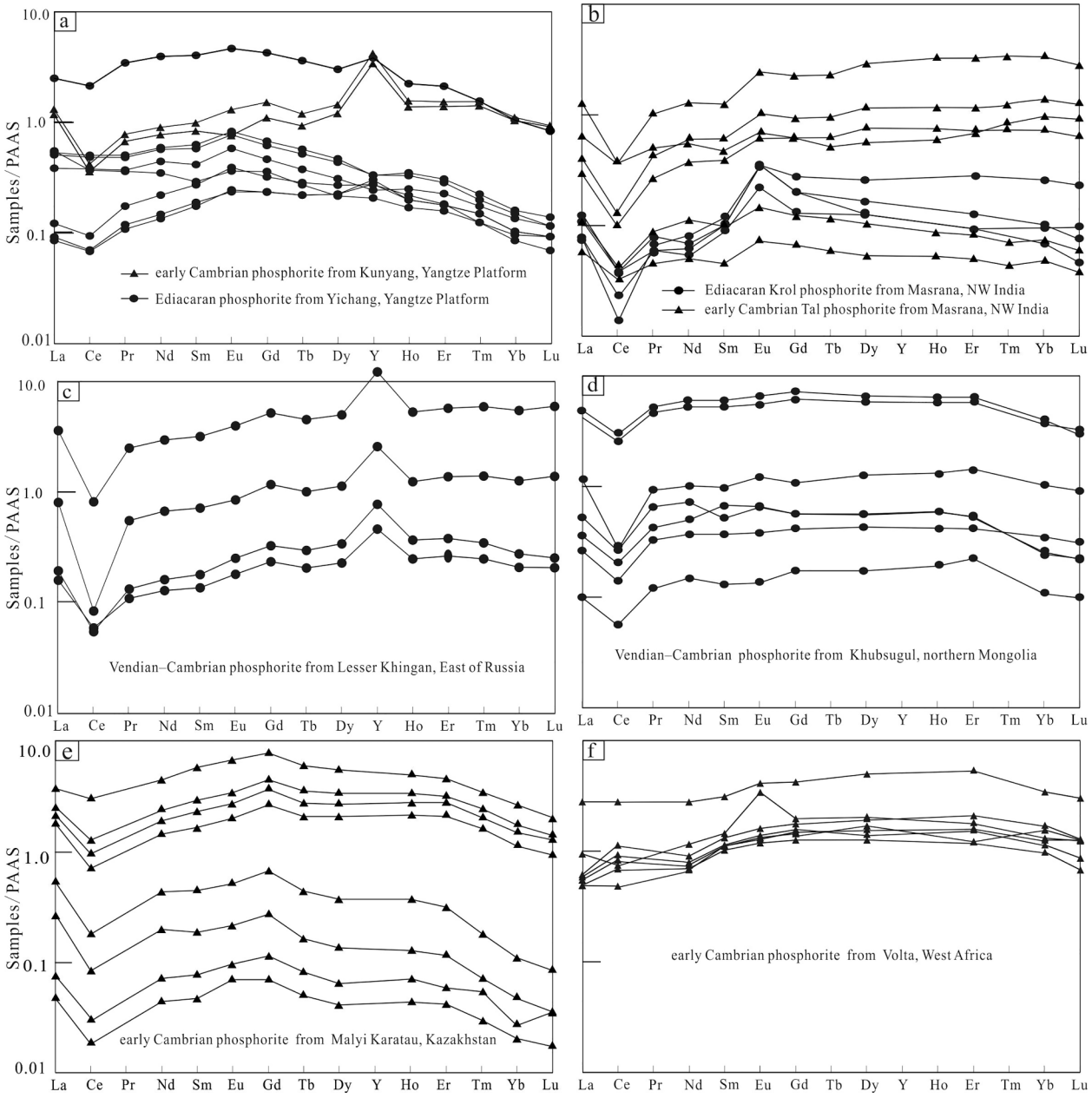

Fig. 15. PAAS-normalized REE + Y distributions of typical old phosphorites around the world. a: Yichang and Kunyang phosphorite from Xin et al. (2015) and Chen et al. (2013), respectively; b: Masrana phosphorite from Khan et al. (2016) and Mazumdar et al. (1999); c: Lesser Khingan phosphorite from Cherepanov et al. (2019); d: Khubsugul phosphorite from Ilyin (1998); e: Malyi Karatau phosphorite from Stammeier et al. (2019); f: Volta phosphorite from Flicoteaux and Trompette (1998).

worldwide, typically in Asia, North America, Australia, Europe, and Africa (Cook, 1992; Ilyin, 1998). Some typical phosphorite deposits were compared based on their REE + Y compositions (Fig. 15a–f).

1) In China, old phosphorite is distributed mainly in the Yangtze Platform. Phosphorites in Yichang, Hubei are hosted in the Ediacaran Doushantuo Formation; phosphorites in Kunyang, Yunnan are hosted in the early Cambrian Meishucun Formation. Yichang phosphorite has ∑REE + Y ranging from 2.17 to 496.70 ppm, weakly negative Ce anomalies, positive Eu anomalies, and right-inclined patterns with HREE depletion (Fig. 15a) (Xin et al., 2015). Kunyang phosphorite has ∑REE + Y ranging from 220.10 to 261.72 ppm, negative Ce anomalies, positive La, Gd, and Y anomalies, and seawater-like REE patterns (Fig. 15a) (Chen et al., 2013).
2) Masrana sedimentary phosphorite, located in the Lesser Himalaya region of North-Western India, belongs to the Ediacaran Upper Krol Formation and the Lower Cambrian Lower Tal Group(Mazumdar and Banerjee, 1998). The phosphorite has ∑REE + Y of 8.02–321.58 ppm, negative Ce anomalies, positive Eu anomalies, weakly positive La and Gd anomalies, and no HREE depletion (Mazumdar et al., 1999; Khan et al., 2016). The PAAS-normalized REE + Y patterns of the Masrana phosphorite show seawater-like patterns, except for HREE enrichment (Fig. 15b) (Mazumdar et al., 1999; Khan et al., 2016).
3) Lesser Khingan phosphorite, located far east of Russia, occurs in the Murandav Formation of the Vendian (equal to Ediacaran–Cambrian). The phosphorite has ∑REE + Y varying from 17.64 to 813.58 ppm, negative Ce anomalies, positive La, Gd, and Y anomalies, and seawater-like REE + Y patterns (Fig. 15c) (Cherepanov et al., 2019).
4) Khubsugul phosphorite, located west of Lake Khubsugul in northern Mongolia, is hosted in Vendian-early Cambrian dolomite (Ilyin, 1998). The phosphorite has ∑REE + Y ranging from 15 to 650 ppm, negative Ce anomalies, weakly positive La and Gd anomalies, and almost flat patterns with HREE depletion (Fig. 15d) (Ilyin, 1998).
5) Malyi Karatau phosphorite, located in South-east Kazakhstan and the north-western part of the Central Asian Tian Shan Mountains, is hosted in the Chuluktau Formation, early Cambrian (Weber et al., 2013). The phosphorite has average ∑REE + Y values of 282 ppm, negative Ce anomalies, positive La and Gd anomalies, and MREE-enriched patterns with HREE depletion (Fig. 15e) (Stammeier et al., 2019).
6) Volta phosphorite, located in the cratonic Taoudeni Basin, West Africa, is hosted in the early Cambrian. The phosphorite has ∑REE + Y ranging from 108.80 to 506.74 ppm, weakly negative to largely positive Ce anomalies, positive Eu anomalies, and flat to moderate concave-down pattern with MREE enrichment and HREE depletion (Fig. 15f) (Flicoteaux and Trompette, 1998).

5.2.2.2. Contrasts of "old phosphorite" around the world. Researchers have suggested that REE + Y patterns are time specific, meaning that phosphorites formed during the same geologic time exhibit similar REE + Y composition on a global scale(Jarvis et al., 1994; Emsbo et al., 2015). However, Shields and Webb (2004) proposed that seawater REE patterns have hardly changed throughout the Phanerozoic considering that authigenic minerals retained REE patterns similar to present-day seawater. Hence, the deviation of sediment patterns from that ofpresent day seawater indicate post-depositional alteration (Elderfield and Pagett, 1986; Wright et al., 1987; Picard et al., 2002). Most old phosphorites share similarities with the phosphorite investigated in this study (Fig. 10), including low ∑REE + Y, no to negative Ce anomalies, and positive La, Gd, and Y anomalies, indicating that they formed under suboxic to oxic conditions, with limited hydrothermal fluids. Nevertheless, the enrichment and depletion of MREE and HREE significantly varied among different deposits, implying that the phosphorites have been subjected to various degrees of post-deposition alteration. The conditions during the diagenetic process, such as redox conditions, position of depositional environment (Grandjean et al., 1987; Lumiste et al., 2021), might have contributed to such differences. It is also noteworthy that the representation of all mineral phases by a mixed dataset of the REE + Y compositions of bulk rocks might have been affected the results. Although REE + Y were redistributed among different minerals in pore water during diagenetic processes, bulk rocks could maintain the REE + Y compositions of all mineral phases. In addition, positive Ce anomalies in Volta phosphorites (Fig. 15f) are related to Ce-enriched iron and manganese phases (Flicoteaux and Trompette, 1998). Accordingly, in situ REE + Y compositions of apatites are crucial for comparison between old and recent apatites, which is equally important in old apatite comparisons.

6. Conclusions

We conducted in situ analyses of apatites from old phosphorite and compared old and recent apatitic grains, as well as typical old phosphorites worldwide. The results may provide valuable insight into REE alteration in the diagenetic process of phosphorite formation.

1) The PAAS-normalized REE + Y distribution patterns of old apatites from Central Guizhou differed among apatites from different stratum. Apatites from the Lower Doushantuo are characterized by left-inclined patterns, with moderately positive La, Gd, and Y anomalies. Apatites from the Upper Doushantuo are characterized by shale-like patterns, with weak enrichment of MREE, slightly negative Ce anomalies, and moderately positive La, Gd, and Y anomalies. Apatites from the Gezhongwu Formation are characterized by "hat-shaped" REE + Y patterns, with notable enrichment of MREEs and evident depletion of HREEs, remarkable negative Ce anomalies, and positive La, Gd, and Y anomalies. In addition, biodetritus grains have REE-enriched outer rims compared to their inner parts, whereas authigenic grains have relatively homogeneous REE + Y distributions. These REE + Y geochemical characteristics indicate that old phosphorite could have been subjected to diagenesis to a certain degree, during which apatites were recrystallized and REE + Y were redistributed in apatites. In contrast, apatites formed under anoxic conditions underwent less diagenetic uptake, maintaining the initial REE + Y characteristics of seawater. Apatites formed under suboxic to oxic conditions adsorbed MREEs from surrounding environment during diagenesis.
2) Compared with recent apatites, old apatites have similar negative Ce anomalies, indistinctive Eu anomalies, and positive La, Gd, and Y anomalies. However, old apatites had depleted HREE and lie in the diagenetic area in the Y/Ho vs Sm_N/Yd_N plot. These similarities and differences between old apatites and recent apatitic grains might imply a similar formation process, with old apatites being additionally subjected to diagenetic modification over long geologic periods. Accordingly, recent apatitic grains could serve as the predecessors of old apatites.
3) Compared with typical old phosphorites around the world, the REE + Y compositions of the studied phosphorites are significantly variable. This indicates that contemporaneous phosphorites preserve differences in depositional conditions and diagenetic alteration among deposits in different locations. Generally, old phosphorite formed under suboxic to oxic conditions, with limited influence from hydrothermal fluids. In addition, the phosphorite underwent various degrees of diagenesis and weathering, during which REE + Y were redistributed and HREE depleted in apatites.

Declaration of Competing Interest

The authors declare that they have no known competing financial interests or personal relationships that could have appeared to influence the work reported in this paper.

Acknowledgments

The authors are grateful to Pro. Min Zeng, Prof. Can Rao, and Dr. Qinping Tan for their helpful suggestions toward improving the quality of this manuscript. This work was supported by the National Natural Science Foundation of China [grant numbers 9206220039, 41972095, 41872251] and United Foundation of National Natural Science Foundation of China [grant number U181240004].

The authors would like to thank all the reviewers who participated in the review and MJEditor (www.mjeditor.com) for its linguistic assistance during the preparation of this manuscript.

Appendix A. Supplementary data

Supplementary data to this article can be found online at https://doi.org/10.1016/j.oregeorev.2022.104813.

References

Alibo, D.S., Nozaki, Y., 1999. Rare earth elements in seawater: Particle association, shale-normalization, and Ce oxidation. Geochim. Cosmochim. Acta 63, 363–372.
Anders, E., Grevesse, N., 1989. Abundances of the elements: meteoritic and solar. Geochim. Cosmochim. Acta 53, 197–214.
Baar, H.J.W.D., Bacon, M.P., Brewer, P.G., Bruland, K.W., 1985. Rare earth elements in the Pacific and Atlantic Oceans. Geochim. Cosmochim. Acta 49, 1943–1959.
Bau, M., 1996. Controls on the fractionation of isovalent trace elements in magmatic and aqueous systems: Evidence from Y/Ho, Zr/Hf, and lanthanide tetrad effect. Contrib. Mineral Petr. 123, 323–333.
Bau, M., Balan, S., Schmidt, K., Koschinsky, A., 2010. Rare earth elements in mussel shells of the Mytilidae family as tracers for hidden and fossil high-temperature hydrothermal systems. Earth Planet Sci. Lett. 299, 310–316.
Bau, M., Dulski, P., 1996. Distribution of yttrium and rare-earth elements in the Penge and Kuruman iron-formations, Transvaal Supergroup, South Africa. Precambr. Res. 79, 37–55.
Bau, M., Dulski, P., 1999. Comparing yttrium and rare earths in hydrothermal fluids from the Mid-Atlantic Ridge: implications for Y and REE behaviour during near-vent mixing and for the Y/Ho ratio of Proterozoic seawater. Chem. Geol. 155, 70–90.
Bau, M., Dulski, P., Möller, P., 1995. Yttrium and holmium South Pacific seawater: vertical distribution and possible fractionation mechanisms. Chem. Erde-Geochem. 55, 1–16.
Bau, M., Koschinsky, A., 2009. Oxidative scavenging of cerium on hydrous Fe oxide: Evidence from the distribution of rare earth elements and yttrium between Fe oxides and Mn oxides in hydrogenetic ferromanganese crusts. Geochem. J. 43, 37–47.
Bau, M., Koschinsky, A., Dulski, P., Hein, J.R., 1996. Comparison of the partitioning behaviours of yttrium, rare-eatrh elements, and titanium between hydrogenetic marine ferromangaese crust ans seawater. Geochim. Cosmochim. Acta 60, 1709–1725.
Bau, M., Möller, P., Dulski, P., 1997. Yttrium and lanthanides in eastern Mediterranean seawater and their fractionation during redox-cycling. Mar. Geol. 56, 123–131.
Bright, C.A., Cruse, A.M., Lyons, T.W., MacLeod, K.G., Glascock, M.D., Ethington, R.L., 2009. Seawater rare-earth element patterns preserved in apatite of Pennsylvanian conodonts? Geochim. Cosmochim. Acta 73, 1609–1624.
Byrne, R.H., Kim, K.H., 1990. Rare earth element scavenging in seawater. Geochim. Cosmochim. Acta 55, 2645–2656.
Byrne, R.H., Liu, X.W., Schijf, J., 1996. The influence of phosphate coprecipitation on rare earth distributions in natural waters. Geochim. Cosmochim. Acta 60, 3341–3346.
Cai, Y.P., Xiao, S.H., Li, G.S., Hua, H., 2019. Diverse biomineralizing animals in the terminal Ediacaran Period herald the Cambrian explosion. Geology 47, 380–384.
Chen, D.F., Dong, W.Q., Qi, L., Chen, G.Q., Chen, X.P., 2003. Possible REE constraints on the depositional and diagenetic environment of Doushantuo Formation phosphorites containing the earliest metazoan fauna. Chem. Geol. 201, 103–118.
Chen, J., Algeo, T.J., Zhao, L., Chen, Z.-Q., Cao, L., Zhang, L., Li, Y., 2015. Diagenetic uptake of rare earth elements by bioapatite, with an example from Lower Triassic conodonts of South China. Earth Sci. Rev. 149, 181–202.
Chen, J.Y., Yang, R.D., Wei, H.R., Gao, J.B., 2013. Rare earth element geochemistry of Cambrian phosphorites from the Yangtze Region. Rare earth element geochemistry of Cambrian phosphorites from the Yangtze Region 31, 101–112.
Chen, W.X., Zhou, F., Wang, H.Q., Zhou, S., Yan, C.J., 2019. The Occurrence States of Rare Earth Elements Bearing Phosphorite Ores and Rare Earth Enrichment Through the Selective Reverse Flotation. Minerals 9, article # https://doi.org/10.3390/min9110698.
Cherepanov, A.A., Berdnikov, N.V., Shtareva, A.V., 2019. Rare earth elements and precise metals in phosphorites of the Gremuchy outcrop, Lesser Khingan, Far East of Russia. Russ. J. Pac. Geol. 38, 99–107.
Cherniak, D.J., 2000. Rare earth element diffusion in apatite. Rare earth element diffusion in apatite 64, 3871–3885.
Chew, D.M., Babechuk, M.G., Cogné, N., 2016. (LA, Q)-ICPMS trace-element analyses of Durango and McClure Mountain apatite and implications for making natural LA-ICPMS mineral standards. Chem. Geol. 435, 35–48.
Cook, P.J., 1992. Phosphogenesis around the Proterozoic Phanerozoic transition. J. Geol. Soc. 149, 615–620.
Cook, P.J., Shergold, J.H., 1984. Phosphorus, phosphorites and skeletal evolution at the Precambrian—Cambrian boundary. Nature 308, 231–236.
Deng, K.Y., Bo, W.U., Luo, M.X., Luo, C., Long, J.X., 2015. Phosphate Rock Geochemistry of the Doushantuo Formation in Shuangshanping, Kaiyang of Guizhou Province and its Genetic Significance. Geology & Exploration 51, 123–132 in Chinese with English abstract.
Deng, Y.N., Ren, J.B., Guo, Q.J., Cao, J., Wang, H.F., Liu, C.H., 2017. Rare earth element geochemistry characteristics of seawater and porewater from deep sea in western Pacific. Sci. Rep-UK 7, article # https://doi.org/10.1038/s41598-41017-16379-41591.
Douville, E., Bienvenu, P., Charlou, J.L., Donval, J.P., Fouquet, Y., Appriou, P., Gamo, T., 1999. Yttrium and rare earth elements in fluids from various deep-sea hydrothermal systems. Geochim. Cosmochim. Acta 63, 627–643.
Elderfield, H., Greaves, M., 1982. The rare earth elements in seawater. Nature 296, 214–219.
Elderfield, H., Pagett, R., 1986. Rare earth elements in ichthyoliths: Variations with redox conditions and depositional environment. Sci. Total Environ. 49, 175–197.
Elderfield, H., Sholkovitz, E.R., 1987. Rare earth elements in the pore waters of reducing nearshore sediments. Earth Planet Sci. Lett. 82, 280–288.
Emsbo, P., McLaughlin, P.I., Breit, G.N., Bray, E.A.B., Koenig, A.E., 2015. Rare earth elements in sedimentary phosphate deposits: Solution to the global REE crisis? Gondwana Res. 27, 776–785.
Fan, H.F., Wen, H.J., Zhu, X.K., 2016. Marine Redox Conditions in the Early Cambrian Ocean: Insights from the Lower Cambrian Phosphorite Deposits. South China. J. Earth Sci. 27, 282–296.
Fan, H.F., Zhu, X.K., Wen, H.J., Yan, B., Li, J., Feng, L.J., 2014. Oxygenation of Ediacaran Ocean recorded by iron isotopes. Geochim. Cosmochim. Acta 140, 80–94.
Filippelli, G.M., 2008. The global phosphorus cycle: Past, present, and future. Elements 4, 89–95.
Filippelli, G.M., Delaney, M.L., 1992. Similar phosphorus fluxes in ancient phosphorite deposits and a modern phosphogenic environment. Geology 20, 709–712.
Flicoteaux, R., Trompette, R., 1998. Cratonic and foreland Early Cambrian phosphorites of West Africa: palaeoceanographical and climatical contexts. Paleogeogr. Palaeocl. 139, 107–120.
Föllmi, K.B., 1996. The phosphorus cycle, phosphogenesis and marine phosphate-rich deposits. Earth Sci. Rev. 40, 55–124.
Fox, D., 2016. What sparked the Cambrian explosion? Nature 530, 268–270.
Frohlich, P.N., Kim, K.H., Jahnke, R., Burnett, W.C., Soutar, A., Deakin, M., 1983. Pore water fluoride in Peru continental margin sediments: Uptake from seawater. Geochim. Cosmochim. Acta 47, 1605–1612.
Goldstein, S.J., Jacobsen, S.B., 1988. Rare earth elements in river waters. Earth Planet. Sci. Lett. 89, 35-47.
Grandjean, P., Cappetta, H., Michard, A., Albare'de, F., 1987. The assessment of REE patterns and $^{143}Nd/^{144}Nd$ ratios in fish remains. The assessment of REE patterns and $^{143}Nd/^{144}Nd$ ratios in fish remains 84, 181-196.
Gunnars, A., Blomqvist, S., Martinsson, C., 2004. Inorganic formation of apatite in brackish seawater from the Baltic Sea: an experimental approach. Mar. Geol. 91, 15–26.
Guo, H.Y., Xia, Y., He, S., Xie, Z.J., Wei, D.T., Lei, B., 2017. Geochemical Characteristics of Zhijin Phosphorite Type Rare-earth Deposit, Guizhou Province, China. Acta Mineralogica Sinica 37, 755–763 in Chinese with English abstract.
Guo, Q.J., Yang, W.D., Liu, C.Q., Strauss, H., Wang, X.L., 2003. Sedimentary Geochemistry Research on the Radiation of Weng'an Biota and the Formation of the Phosphorite Ore Deposit, Guizhou. Bulletin of Mineralogy Petrology & Geochemistry 22, 11–17 in Chinese with English abstract.
Haley, B.A., Klinkhammer, G.P., McManus, J., 2004. Rare earth elements in pore waters of marine sediments. Geochim. Cosmochim. Acta 68, 1265–1279.
Herwartz, D., Tutken, T., Jochum, K.P., Sander, P.M., 2013. Rare earth element systematics of fossil bone revealed by LA-ICPMS analysis. Rare earth element systematics of fossil bone revealed by LA-ICPMS analysis 103, 161–183.
Holser, W.T., 1997. Evaluation of the application of rare-earth elements to paleoceanography. Paleogeogr. Palaeocl. 132, 309–323.
Huldtgren, T., Cunningham, J.A., Yin, C.y., Stampanoni, M., Marone, F., Donoghue, P.C. J., Bengtson, S., 2011. Fossilized Nuclei and GerminationStructures Identify Ediacaran "Animal Embryos" as Encysting Protists. Science 6063, 1696–1699.
Igisu, M., Komiya, T., Kawashima, M., Nakashima, S., Ueno, Y., Han, J., Shu, D., Li, Y., Guo, J., Maruyama, S., Takai, K., 2014. FTIR microspectroscopy of Ediacaran phosphatized microfossils from the Doushantuo Formation, Weng'an. South China. Gondwana Res. 25, 1120–1138.
Ilyin, A.V., 1998. Rare-earth geochemistry of 'old' phosphorites and probability of syngenetic precipitation and accumulation of phosphate. Chem. Geol. 144, 243–256.
Ingall, E.D., Vancappellen, P., 1990. Relations between sedimentation-rate and burial of organic phosphorus and organic-carbon in marine-sediments. Geochim. Cosmochim. Acta 54, 373–386.
Jahnke, R.A., 1984. The synthesis and solibility of carbonate fluorapatite. Am. J. Sci. 284, 58–78.
Jarvis, I., Burnett, W.C., Nathan, Y., Almbaydin, F.S.M., Attia, A.K.M., Castro, L.N., Flicoteaux, R., Hilmy, M.E., Husain, V., Qutawnah, A.A., Serjani, A., Zanin, Y.N., 1994. Phosphorite geochemistry—state-of-the-art and environmental concern. Eclogae Geologicae Helvetiae 87, 643–700.
Jiang, G.Q., Shi, X.Y., Zhang, S.H., Wang, Y., Xiao, S.H., 2011. Stratigraphy and paleogeography of the Ediacaran Doushantuo Formation (ca. 635–551 Ma) in South China. Gondwana Res. 19, 831–849.

Jiang, S.Y., Yang, J.H., Ling, H.F., Chen, Y.Q., Feng, H.Z., Zhao, K.D., Ni, P., 2007a. Extreme enrichment of polymetallic Ni–Mo–PGE–Au in Lower Cambrian black shales of South China: An Os isotope and PGE geochemical investigation. Paleogeogr. Palaeocl. 254, 217–228.

Jiang, S.Y., Zhao, H.X., Chen, Y.-Q., Yang, T., Yang, J.-H., Ling, H.-F., 2007b. Trace and rare earth element geochemistry of phosphate nodules from the lower Cambrian black shale sequence in the Mufu Mountain of Nanjing, Jiangsu province. China. Chem. Geol. 244, 584–604.

Joosu, L., Lepland, A., Kreitsmann, T., Upraus, K., Roberts, N.M.W., Paiste, P., Martin, A. P., Kirsimae, K., 2016. Petrography and the REE-composition of apatite in the Paleoproterozoic Pilgujarvi Sedimentary Formation, Pechenga Greenstone Belt. Russia. Geochim. Cosmochim. Acta 186, 135–153.

Joshi, S.R., Kukkadapu, R.K., Burdige, D.J., Bowden, M.E., Sparks, D.L., Jaisi, D.P., 2015. Organic Matter Remineralization Predominates Phosphorus Cycling in the Mid-Bay Sediments in the Chesapeake Bay Environ. Sci. Technol. 49, 5887–5896.

Khan, S.A., Khan, K.F., Dar, S.A., 2016. REE geochemistry of Early Cambrian phosphorites of Masrana and Kimoi blocks, Uttarakhand, India. Arab. J. Geosci. 9, article # https://doi.org/10.1007/s12517-12016-12477-12518.

Kidder, D.L., Krishnaswamy, R., Mapes, R.H., 2003. Elemental mobility in phosphatic shales during concretion growth and implications for provenance analysis. Chem. Geol. 198, 335–353.

Knudsen, A.C., Gunter, M.E., 2002. Sedimentary phosphorites – An example: Phosphoria formation, southeastern Idaho, USA, In: Kohn M.J., Rakovan J., Hughes J.M. (Eds.), Phosphates: Geochemical, Geobiological, and Materials Importance. 363-389 pp.

Kocsis, L., Gheerbrant, E., Mouflih, M., Cappetta, H., Ulianov, A., Chiaradia, M., Bardet, N., 2016. Gradual changes in upwelled seawater conditions (redox, pH) from the late Cretaceous through early Paleogene at the northwest coast of Africa: Negative Ce anomaly trend recorded in fossil bio-apatite. Gradual changes in upwelled seawater conditions (redox, pH) from the late Cretaceous through early Paleogene at the northwest coast of Africa: Negative Ce anomaly trend recorded in fossil bio-apatite 421, 44-54.

Kocsis, L., Trueman, C.N., Palmer, M.R., 2010. Protracted diagenetic alteration of REE contents in fossil bioapatites: Direct evidence from Lu-Hf isotope systematics. Protracted diagenetic alteration of REE contents in fossil bioapatites: Direct evidence from Lu-Hf isotope systematics 74, 6077-6092.

Kohn, M.J., 2008. Models of diffusion-limited uptake of trace elements in fossils and rates of fossilization. Models of diffusion-limited uptake of trace elements in fossils and rates of fossilization 72, 3758-3770.

Lécuyer, C., Reynard, B., Grandjean, P., 2004. Rare earth element evolution of Phanerozoic seawater recorded in biogenic apatites. Chem. Geol. 204, 63–102.

Liao, J.L., Sun, X.M., Li, D.F., Sa, R.N., Lu, Y., Lin, Z.Y., Xu, L., Zhan, R.Z., Pan, Y.G., Xu, H.F., 2019. New insights into nanostructure and geochemistry of bioapatite in REE-rich deep-sea sediments: LA-ICP-MS, TEM, and Z-contrast imaging studies. Chem. Geol. 512, 58–68.

Liu, B.J., Xu, X.S., Xu, Q., Pan, X.N., Huang, H.Q., 1993. Sedimentary crustal evolution and mineralization of palaeocontinent in South China. Scientific Publications, Beijing (in Chinese).

Liu, K.W., 1989. The evolution of apatite inerals in the diagenetic processes. Acta Mineralogica Sinica 4, 310-323+385-386 (in Chinese with English abstract).

Liu, X.Q., Zhang, H., Tang, Y., Long, L.Y., 2020. REE Geochemical Characteristic of Apatite: Implications for Ore Genesis of the Zhijin Phosphorite. Minerals 10, article # https://doi.org/10.3390/min10111012.

Liu, Y.S., Hu, Z.C., Gao, S., Günther, D., Xu, J., Gao, C.G., Chen, H.H., 2008. In situ analysis of major and trace elements of anhydrous minerals by LA-ICP-MS without applying an internal standard. Chem. Geol. 257, 34–43.

Lumiste, K., Lang, L., Paiste, P., Lepland, A., Kirsimäe, K., 2021. Heterogeneous REE + Y distribution in Early Paleozoic shelly phosphorites: Implications for enrichment mechanisms. Heterogeneous REE + Y distribution in Early Paleozoic shelly phosphorites: Implications for enrichment mechanisms 586, article # https://doi.org/10.1016/j.chemgeo.2021.120590.

Lumiste, K., Mänd, K., Bailey, J., Paiste, P., Lang, L., Lepland, A., Kirsimäe, K., 2019. REE +Y uptake and diagenesis in Recent sedimentary apatites. Chem. Geol. 525, 268–281.

Marshall, C.R., 2006. Explaining the Cambrian "explosion" of animals. Annu. Rev. Earth P. L. Sc. 34, 355-384.

Martinez-Ruiz, F., Ortega-Huertas, M., Palomo, I., 1999. Positive Eu anomaly development during diagenesis of the K/T boundary ejecta layer in the Agost section (SE Spain): implications for trace-element remobilization. Terra Nova 11, 290–296.

Mazumdar, A., Banerjee, D.M., 1998. Siliceous sponge spicules in the Early Cambrian chert-phosphorite member of the Lower Tal Formation, Krol belt, Lesser Himalaya. Geology 26, 899–902.

Mazumdar, A., Banerjee, D.M., Schidlowski, M., Balaram, V., 1999. Rare-earth elements and Stable Isotope Geochemistry of early Cambrian chert-phosphorite assemblages from the Lower Tal Formation of the Krol Belt (Lesser Himalaya, India). Chem. Geol. 156, 275–297.

McArthur, J.M., Walsh, J.N., 1984. Rare-earth geochemistry of phosphorites. Chem. Geol. 47, 191–220.

McLennan, S.M., 1989. Rare earth elements in sedimentary rocks: influence of provenance and sedimentary processes Rev. Mineral. Geochem. 21, 169–200.

Mi, W.T., 2010. Phosphorites Sedimentary Event in Sinian Doushantuo period, West Yangtze Area – the Cases Study of Weng'an Phosphorite in Guizhou and Yichang Phosphorite in Hubei. (Ph. D Thesis), Chengdu University of Technology, 99 pp (in Chinese with English abstract).

Muscente, A.D., Hawkins, A.D., Xiao, S., 2015. Fossil preservation through phosphatization and silicification in the Ediacaran Doushantuo Formation (South China): a comparative synthesis. Paleogeogr. Palaeocl. 434, 46–62.

Olivarez, A.M., Owen, R.M., 1991. The europium anomaly of seawater: implications for fluvial versus hydrothermal REE inputs to the oceans. Chem. Geol. 92, 317–328.

Ounis, A., Kocsis, L., Chaabani, F., Pfeifer, H.R., 2008. Rare earth elements and stable isotope geochemistry (delta C-13 and delta O-18) of phosphorite deposits in the Gafsa Basin, Tunisia. Rare earth elements and stable isotope geochemistry (delta C-13 and delta O-18) of phosphorite deposits in the Gafsa Basin. Tunisia 268, 1–18.

Oxmann, J.F., Pham, Q.H., Lara, R.J., 2008. Quantification of individual phosphorus species in sediment: a sequential conversion and extraction method. Eur. J. Soil. Sci. 59, 1177–1190.

Oxmann, J.F., Schwendenmann, L., 2014. Quantification of octacalcium phosphate, authigenic apatite and detrital apatite in coastal sediments using differential dissolution and standard addition. Ocean Sci. 10, 571–585.

Papineau, D., 2010. Global Biogeochemical Changes at Both Ends of the Proterozoic: Insights from Phosphorites. Astrobiology 10, 165–181.

Paul, S.A.L., Volz, J.B., Bau, M., Koster, M., Kasten, S., Koschinsky, A., 2019. Calcium phosphate control of REY patterns of siliceous-ooze-rich deep-sea sediments from the central equatorial Pacific. Geochim. Cosmochim. Acta 251, 56–72.

Picard, S., Lécuyer, C., Barrat, J.A., Garcia, J.P., Dromart, G., Sheppard, S.M.F., 2002. Rare earth element contents of Jurassic fish and reptile teeth and their potential relation to seawater composition (Anglo-Paris Basin, France and England). Chem. Geol. 186, 1–16.

Planavsky, N.J., Rouxel, O.J., Bekker, A., Lalonde, S.V., Konhauser, K.O., Reinhard, C.T., Lyons, T.W., 2010. The evolution of the marine phosphate reservoir. Nature 467, 1088–1090.

Pourret, O., Davranche, M., Gruau, G., Dia, A., 2008. New insights into cerium anomalies in organic-rich alkaline waters. Chem. Geol. 251, 120–127.

Pufahl, P.K., Groat, L.A., 2017. Sedimentary and igneous phosphate deposits: formation and exploration: An invited Paper. Econ. Geol. 112, 483–516.

Pufahl, P.K., Hiatt, E.E., 2012. Oxygenation of the Earth's atmosphere-ocean system: A review of physical and chemical sedimentologic responses. Mar. Petrol. Geol. 32, 1–20.

Reynard, B., Lécuyer, C., Grandjean, P., 1999. Crystal-chemical controls on rare-earth element concentrations in fossil biogenic apatites and implications for paleoenvironmental reconstructions. Chem. Geol. 155, 233–241.

Ruttenberg, K.C., Berner, R.A., 1993. Authigenic apatite formation and burial in sediments from non-upwelling, continental margin environments. Authigenic apatite formation and burial in sediments from non-upwelling, continental margin environments 57, 991-1007.

She, Z.B., Strother, P., McMahon, G., Nittler, L.R., Wang, J.H., Zhang, J.H., Sang, L.K., Ma, C.Q., Papineau, D., 2013. Terminal Proterozoic cyanobacterial blooms and phosphogenesis documented by the Doushantuo granular phosphorites I: In situ micro-analysis of textures and composition. Precambr. Res. 235, 20–35.

Shi, C.H., 2005. Formation of phosphorite deposit, Breakup of Rodinia supercontinent and Biology explosion- A case study of Weng'an, Kaiyang and Zhijin phosphorite deposits of Guizhou Province. (Ph. D. thesis), University of Chinese Academy of Sciences, 108 pp (in Chinese with English abstract).

Shields, G., Stille, P., 2001. Diagenetic constraints on the use of cerium anomalies as palaeoseawater redox proxies: an isotopic and REE study of Cambrian phosphorites. Chem. Geol. 175, 29–48.

Shields, G.A., Webb, G.E., 2004. Has the REE composition of seawater changed over geological time? Has the REE composition of seawater changed over geological time? 204, 103-107.

Skinner, L.C., Sadekov, A., Brandon, M., Greaves, M., Plancherel, Y., de la Fuente, M., Gottschalk, J., Souanef-Ureta, S., Sevilgen, S., Scrivner, A.E., 2019. Rare Earth Elements in early-diagenetic foraminifer 'coatings': Pore-water controls and potential palaeoceanographic applications. Geochim. Cosmochim. Acta 245, 118–132.

Stammeier, J.A., Hippler, D., Nebel, O., Leis, A., Grengg, C., Mittermayr, F., Kasemann, S. A., Dietzel, M., 2019. Radiogenic Sr and Stable C and O Isotopes Across Precambrian-Cambrian Transition in Marine Carbonatic Phosphorites of Malyi Karatau (Kazakhstan)-Implications for Paleo-environmental Change. Geochem. Geochem. Geosy. 20, 3–23.

Steiner, M., Wallis, E., Ertman, B.D., Zhao, Y.L., Yang, R.D., 2001. Submarine hydrothermal exhalative ore layers in black shales from South China and associated fossils insights into Lower Cambrian facies and bio-evolution. Paleogeogr. Palaeocl. 169, 165–169.

Takahashi, Y., Hayasaka, Y., Morita, K., Kashiwabara, T., Nakada, R., Marcus, M.A., Kato, K., Tanaka, K., Shimizu, H., 2015. Transfer of rare earth elements (REE) from manganese oxides to phosphates during early diagenesis in pelagic sediments inferred from REE patterns, X-ray absorption spectroscopy, and chemical leaching method. Geochem. J. 49, 653–674.

Taylor, S.R., McLennan, S.M., 1985. The Continental Crust: Its Composition and Evolution, An Examination of the Geochemical Record Preserved in Sedimentary Rocks. Blackwell Scientific Publications, Oxford, p. 312.

Trotter, J.A., Barnes, C.R., McCracken, A.D., 2016. Rare earth elements in conodont apatite: Seawater or pore-water signatures? Paleogeogr. Palaeocl. 462, 92–100.

Trueman, C.N., Benton, M.J., Palmer, M.R., 2003. Geochemical taphonomy of shallow marine vertebrate assemblages. Geochemical taphonomy of shallow marine vertebrate assemblages 197, 151–169.

Trueman, C.N., Kocsis, L., Palmer, M.R., Dewdney, C., 2011. Fractionation of rare earth elements within bone mineral: A natural cation exchange system. Fractionation of rare earth elements within bone mineral: A natural cation exchange system 310, 124–132.

Trueman, C.N., Tuross, N., 2002. Trace elements in recent and fossil bone apatite. Conference on Phosphates – Geochemical, Geobiological and Materials Importance. Reviews in Mineralogy & Geochemistry. 48: 489-521.

Weber, B., Steiner, M., Evseev, S., Yergaliev, G., 2013. First report of a Meishucun-type early Cambrian (Stage 2) ichnofauna from the Malyi Karatau area (SE Kazakhstan): Palaeoichnological, palaeoecological and palaeogeographical implications. Paleogeogr. Palaeocl. 392, 209–231.

Wen, H.J., Carignan, J., Zhang, Y.X., Fan, H.F., Cloquet, C., Liu, S.R., 2011. Molybdenum isotopic records across the Precambrian-Cambrian boundary. Geology 39, 775–778.

Wright, J., Schrader, H., Holser, W.T., 1987. Paleoredox variations in ancient oceans recorded by rare earth elements in fossil apatite. Geochim. Cosmochim. Acta 51, 631–644.

Wu, K., Ma, D.S., Pan, J.Y., Nie, W.M., Zhou, J., Xia, F., Liu, L., 2006. The Geochemistry of Phosphorite of Doushantuo Formation in Weng'an, China: Insights from Trace Elements and REE. Journal of East China Institute of Technology 29, 108–114 in Chinese with English abstract.

Wu, X.H., Han, Z.J., Cai, J.F., 1999. Guizhou phosphorite. Geological Publishing House, Beijing (in Chinese with English abstract).

Xiao, S.H., Knoll, A.H., 1999. Fossil preservation in the Neoproterozoic Doushantuo phosphorite Lagerstatte, South China. Lethaia 32, 219–240.

Xiao, S.H., Zhang, Y., Knoll, A.H., 1998. Three-dimensional preservation of algae and animal embryos in a Neoproterozoic phosphorite. Nature 391, 553–558.

Xin, H., Jiang, S.Y., Yang, J.H., Wu, H.P., Pi, D.H., 2015. Rare earth element and Sr–Nd isotope geochemistry of phosphatic rocks in Neoproterozoic Ediacaran Doushantuo Formation in Zhangcunping section from western Hubei Province, South China. Paleogeogr. Palaeocl. 440, 712–724.

Xue, Y.S., Cao, R.J., Tang, T.F., Yin, L.M., Yu, C.L., Yang, J.D., 2001. The Sinian stratigraphic sequence of the Yangtze region and correlation to the late Precambrian strata of North China. Journal of stratigraphy 25, 207-216+234 (in Chinese with English abstract).

Yang, H.Y., Xiao, J.F., Xia, Y., Xie, Z.J., Tan, Q.P., Xu, J.B., Guo, H.Y., He, S., Wu, S.W., 2019. Origin of the Ediacaran Weng'an and Kaiyang phosphorite deposits in the Nanhua basin, SW China. J. Asian Earth Sci. 182, article # https://doi.org/10.1016/j.jseaes.2019.103931.

Yang, H.Y., Xiao, J.F., Xia, Y., Xie, Z.J., Tan, Q.P., Xu, J.B., He, S., Wu, S.W., Liu, X.Q., Gong, X.X., 2021a. Phosphorite generative processes around the Precambrian-Cambrian boundary in South China: An integrated study of Mo and phosphate O isotopic compositions. Geosci. Front. 12, article # https://doi.org/10.1016/j.gsf.2021.101187.

Yang, H.Y., Zhao, Z.F., Xia, Y., Xiao, J.F., 2021b. REY enrichment mechanisms in the early Cambrian phosphorite from South China. REY enrichment mechanisms in the early Cambrian phosphorite from South China 426.

Ye, L.J., 1989. Chinese phosphorite rock. Science Press, Beijing. 339 pp (in Chinese).

Ye, Y.T., Wang, H.J., Wang, X.M., Zhai, L.N., Wu, C.D., Zhang, S.C., 2020. Elemental geochemistry of lower Cambrian phosphate nodules in Guizhou Province, South China: An integrated study by LA-ICP-MS mapping and solution ICP-MS. Paleogeogr. Palaeocl. 538, article # https://doi.org/10.1016/j.palaeo.2019.109459.

Yin, L.M., Zhu, M.Y., Knoll, A.H., Yuan, X.L., Zhang, J.M., Hu, J., 2007. Doushantuo embryos preserved inside diapause egg cysts. Nature 446, 661–663.

Yuan, H.Z., Li, Q., Kukkadapu, R.K., Liu, E., Yu, J.H., Fang, H., Li, H., Jaisi, D.P., 2019. Identifying sources and cycling of phosphorus in the sediment of a shallow freshwater lake in China using phosphate oxygen isotopes. Sci. Total Environ. 676, 823–833.

Zhang, J., Amakawa, H., Nozaki, Y., 1994. The comparative behaviors of Yttrium and Lanthanides in the seawater of the North Pacfic. Geophys. Res. Lett. 21, 2677–2680.

Zhang, J., Zhang, Q., Chen, D.L., 2003. REE geochemistry of the Ore-bearing REE in Xinhua phosphorite, Zhijin, Guizhou. Journal of Mineralogy and Petrology 23, 35–38 in Chinese with English abstract.

Zhang, J., Zhang, Q., Chen, D.L., 2004. REE geochemistry of the Xinhua REE – bearing phosphorite deposit, Zhijin County, Guizhou province. Geology and Prospecting 40, 40–44 in Chinese with English abstract.

Zhang, Y.G., Pufahl, P.K., Du, Y.S., Chen, G.Y., Liu, J.Z., Chen, Q.G., Wang, Z.P., Yu, W. C., 2019. Economic phosphorite from the Ediacaran Doushantuo Formation, South China, and the Neoproterozoic-Cambrian Phosphogenic Event. Sediment. Geol. 388, 1–19.

Zhou, C.M., Xie, G.W., McFadden, K., Xiao, S.H., Yuan, X.L., 2007. The diversification and extinction of Doushantuo-Pertatataka acritarchs in South China: causes and biostratigraphic significance. Geol. J. 42, 229–262.

Zhu, B., Jiang, S.Y., 2017. LA-ICP-MS analysis of rare earth elements on phosphatic grains of the Ediacaran Doushantuo phosphorite at Weng'an, South China: implication for depositional conditions and diagenetic processes. Geol. Mag. 154, 1381–1397.

Zhu, M.Y., Zhang, J.M., Yang, A.H., 2007. Integrated Ediacaran (Sinian) chronostratigraphy of South China. Paleogeogr. Palaeocl. 254, 7–61.